



Mineralogical and geochemical characteristics of tonsteins from the Middle Jurassic Yan'an Formation, Ordos Basin, North China



Zihui Zhang^a, Dawei Lv^{a,*}, Chengshan Wang^b, James C. Hower^c, Munira Raji^d, Tiantian Wang^e, Jianqiang Zhang^f, Yi Yang^g

^a Shandong Provincial Key Laboratory of Depositional Mineralization and Sedimentary Minerals, College of Earth Sciences and Engineering, Shandong University of Science and Technology, Qingdao 266590, China

^b School of Earth Sciences and Resources, China University of Geosciences, Beijing 100083, China

^c University of Kentucky, Center for Applied Energy Research, 2540 Research Park Drive, Lexington, KY 40511, United States of America

^d University of Portsmouth, School of the Environment, Geography and Geosciences, St. Michael's Building, White Swan Road, Portsmouth PO1 2DT, United Kingdom

^e Institute of Earth Sciences, China University of Geosciences, Beijing 100083, China

^f General Prospecting Institute of China National Administration of Coal Geology, Beijing 100039, China

^g Anhui Nuclear Exploration Technology Central Institute, Wuhu, Anhui 241000, China

ARTICLE INFO

Keywords:

Ordos Basin

Jurassic

Tonstein

Minerals in coal

Elements in coal

Element mobility

ABSTRACT

Although the Jurassic features a considerable accumulation of coal worldwide, only a few tonsteins within coal seams in this coal-forming period have been investigated. This paper presents the detailed mineralogical and geochemical compositions of six tonstein layers from the Middle Jurassic Yan'an Formation, Ordos Basin, North China. Based on the typical evidence of the distinct field characteristics occurring as paler thin beds with lateral continuity; conchoidal and flint-like fracture planes; sharp contacts with adjacent coals; and the mineralogical compositions, such as vermicular kaolinite, angular quartz, and euhedral zircon crystals with a single U—Pb age peak, the intra-seam clay beds of the Yan'an Formation were determined to have been mainly derived from a significant pyroclastic source. However, rounded quartz, muscovite, and detrital zircon grains in the tonsteins reflect minor contribution of terrigenous debris from sediment source regions. Moreover, a line of geochemical features including low $\text{TiO}_2/\text{Al}_2\text{O}_3$ values, $\text{Al}_2\text{O}_3/\text{TiO}_2\text{-Nb/Yb}$, and $\text{Al}_2\text{O}_3/\text{TiO}_2\text{-Zr/TiO}_2$ diagrams; low REY concentrations with high fractionation between light REE and heavy REY (REY, rare earth elements and Y; REE, rare earth elements); and pronounced negative Eu anomalies, suggest that the tonsteins have a felsic (rhyolitic) magma origin. A systematic geochemical analysis of enclosing coals of the tonsteins was also conducted to determine the leaching behavior of the trace elements from the tonsteins into the enclosing coals. The results show that Th, U, Nb, Ta, Zr, and Hf tend to be enriched in the overlying and underlying coals and have an enrichment width of up to 30 cm. Similarly, the elevated concentrations of Zn, Rb, Cs, Pb, La, Ce, Pr, and Nd only occur in a relatively narrow zone above and below the tonsteins. The width of the enrichment in the enclosing coals may be mainly related to the properties of the tonsteins, e.g., thickness and original volcanogenic material, the characters of elements including mobility and concentration, and the nature of coals, such as coal rank.

1. Introduction

Tonsteins resulting from altered volcanic ashes have been found worldwide in coal-bearing strata (Dai et al., 2011, 2017; Spears, 2012). Typically, the beds are dominantly kaolinite-rich (> 50%) rocks occurring as thin (< 10 cm) but laterally persistent bands within coal seams (Dai et al., 2017 and references therein), which differ from normal mudrocks with a paler color, conchoidal and flint-like fracture plane,

and sharp contact with the adjacent sediments (Spears, 2012). The distinctive appearance of tonsteins has been extensively used as excellent chronostratigraphic markers for identification and correlation of coal seams during exploration and mining programs (e.g., Bohor and Triplehorn, 1993; Burger and Damberger, 1985; Dai et al., 2014a; Hong et al., 2019; Zhou et al., 2000). Furthermore, some of the primary minerals (e.g., zircon, monazite, and sanidine) that survive weathering and alteration in tonsteins can be used for radiometric age

* Corresponding author.

E-mail address: lvdawei95@163.com (D. Lv).

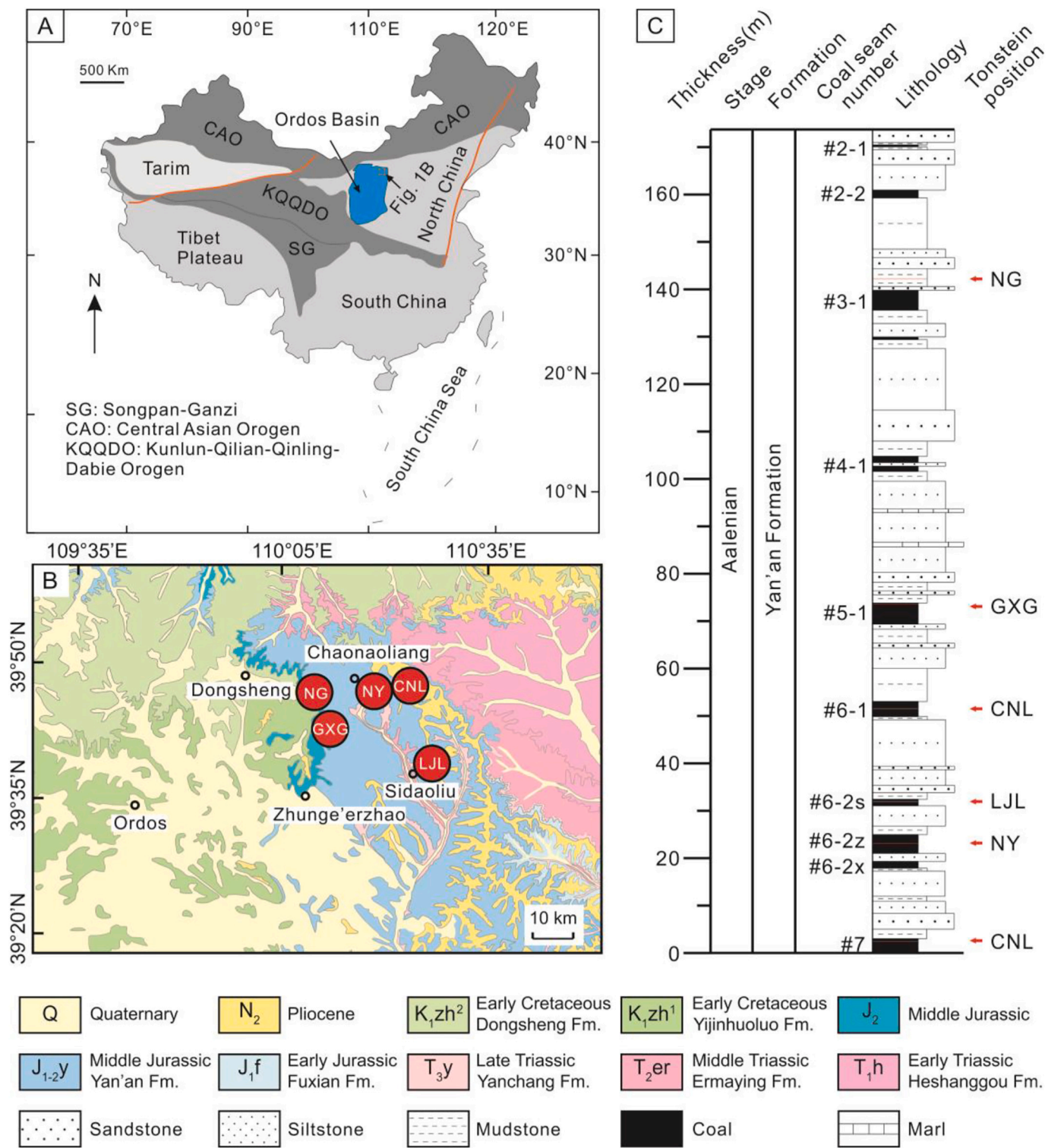


Fig. 1. (A) Generalized tectonic map of China showing the position of the Ordos Basin and the study area (modified from Darby and Ritts, 2002). (B) Geological map of the study area (modified from Zhang et al., 2021) showing the position of the five sampling mine sites. NG-Nangai, GXG-Gaoxigou, NY-Nayuan, CNL-Chao-naoliang, LJJ-Lijialiango. (C) Stratigraphic column of the Yan'an Formation in the Dongsheng Coalfield, Ordos Basin (Zhang et al., 2021), illustrating the lithostratigraphy, coal seam number, and tonstein positions with corresponding names of sampling coal mines.

determination (Guerra-Sommer et al., 2008; Lyons et al., 2006; Rice et al., 1990; Wainman et al., 2015; Zhang et al., 2020, 2021), which is important to provide globally chronostratigraphic calibration and correlation (Dai et al., 2017). Detailed mineralogy and geochemistry of tonsteins may provide indicative information on the depositional conditions, regional tectonic evolution, nature of source magmas, and mass

extinction events in Earth's history (Altaner and Grim, 1990; Dai et al., 2014a, 2014b, 2017; Erkoyun et al., 2019; Hong et al., 2019; Karayigit et al., 2020a, 2020b; Liu et al., 2020; Oskay et al., 2019; Sha et al., 2020; Shen et al., 2021; Spears and Arbuzov, 2019; Wang et al., 2020; Zheng et al., 2020). In addition, tonstein layers can introduce trace elements into the peat by groundwaters or hydrothermal solutions, which may

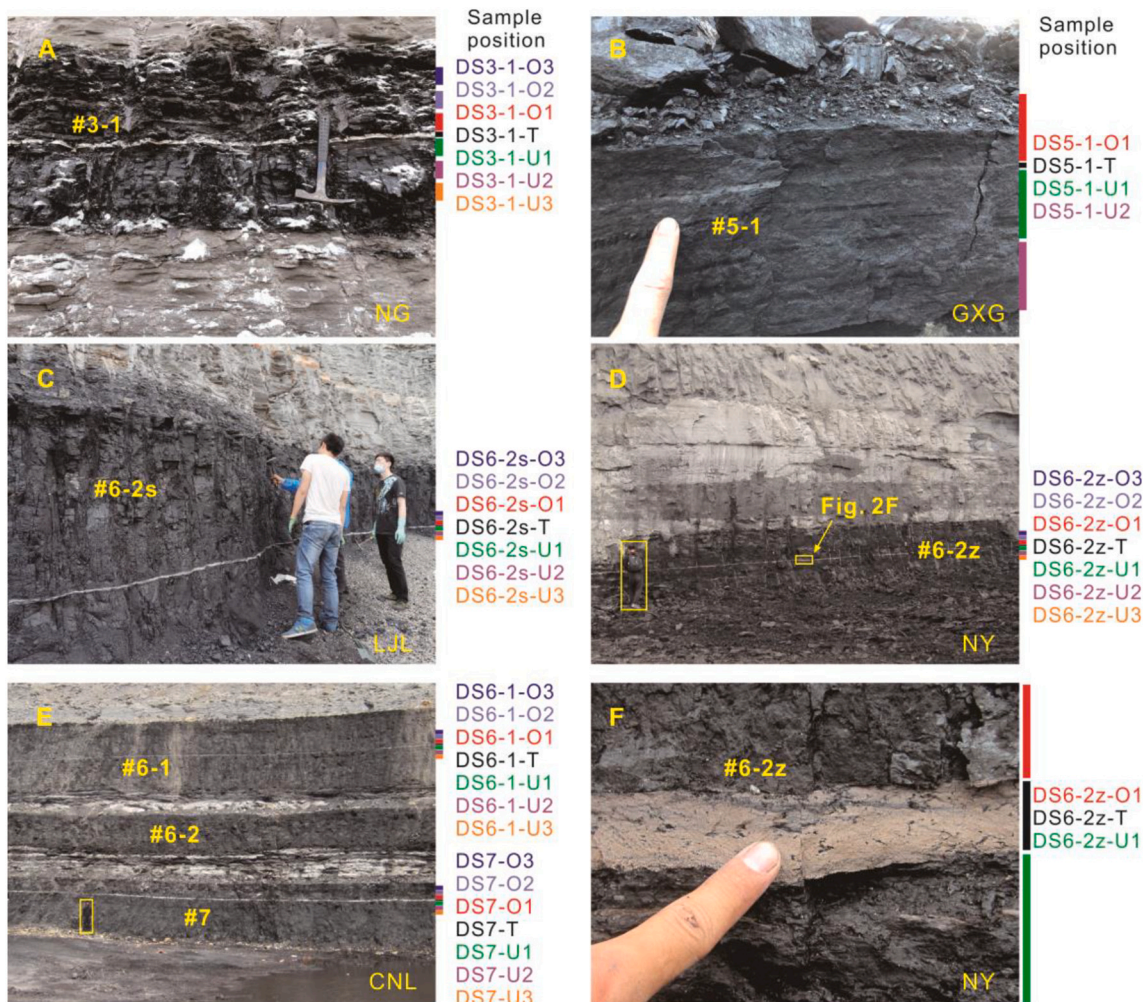


Fig. 2. Field photographs of tonsteins within coal seams. Sample positions of the tonsteins and enclosing coals are shown on the right of the photographs. White thin layers are the tonsteins and black beds are coals.

cause the enrichment of some elements in the underlying or overlying coal benches, and in some cases, resulting in commercial deposits (e.g., Arbuzov et al., 2016, 2018; Crowley et al., 1989; Dai et al., 2003, 2014a, Dai et al., 2010, Dai et al., 2017; Eshkenazy, 2006; Ketris and Yudovich, 2009; Hower et al., 1999; Spears and Arbuzov, 2019; Zhao et al., 2015).

The Jurassic marks an important coal-forming interval in Earth's history, characterized by massive coal-bearing strata widely distributed worldwide, especially in northern China (Boucot et al., 2013). However, a few studies have been carried out on Jurassic tonsteins from Iran (Goodarzi et al., 2006), Russia (Admakin and Portnov, 1987; Arbuzov et al., 2016; Chekin, 1973; Mikheeva et al., 2020), and China (China National Administration of Coal Geology, 1996). Recently, Zhang et al. (2020, 2021) reported the occurrence and age of tonsteins in the Jurassic coals of the Ordos Basin in North China, but the mineral and chemical composition of the beds have not been undertaken. This paper systematically investigates the nature of six tonsteins in the Middle Jurassic coal-bearing strata (Yan'an Formation) in the northeastern margin of the Ordos Basin in North China. Petrographic, mineralogical, and geochemical characteristics of the tonsteins were used to identify a volcanic origin and source. Moreover, the mobility of trace elements during alteration of the volcanic ash was presented based on the enclosing coals.

2. Geological setting

The Ordos Basin is the second largest terrestrial sedimentary basin in

China and contains vast energy resources, such as coal, oil, natural gas, and uranium (Ao et al., 2012). The basin developed on the western margin of the North China-Korean Platform (Fig. 1A), which is mainly Precambrian metamorphic rock basement upon which Cambrian through Middle Ordovician carbonate rocks were deposited. During the Caledonian orogeny, these Lower Paleozoic rocks were directly overlain by alternating marine and terrestrial deposits of the Late Carboniferous-Middle Triassic. After the Late Triassic, the basin entered a period of entirely continental deposition with a series of unconformities due to the Indosinian and Yanshan orogenies. Ultimately, the form of the Ordos Basin is the result of the Late Cenozoic Himalayan orogeny (Johnson et al., 1989).

The Dongsheng Coalfield, located in the northeastern margin of the Ordos Basin, was chosen for this study (Fig. 1B). The Middle Jurassic Yan'an Formation developed in fluvial and deltaic-lacustrine environments consisting of sandstone, siltstone, mudstone, coal, and minor marl, is the principal coal-bearing strata in the Dongsheng Coalfield (Li et al., 1992). It records continuous deposition, disconformably overlies the Lower Jurassic Fuxian Formation or the Upper Triassic Yanchang Formation on a weathered land surface and is disconformably overlain by the fluvial Middle Jurassic-age Zhiluo Formation. The Yan'an Formation varies in thickness from 133 to 279 m and contains six main coal groups labeled #2 to #7 from top to base (each consisting of several coal seams) (Fig. 1C). The bituminous coals of the Yan'an Formation have low ash, low sulfur, and high volatile matter (Wang et al., 2018). The chronostratigraphic analysis shows that all coal seams of the Yan'an

Table 1
Sampling information of six tonsteins.

Sample	Latitude (E)	Longitude (N)	Thickness	Coal mine	Horizon
DS3-1-T	110°10'8.37"	39°47'53.64"	1.3 cm	NG	Above #3-1
DS5-1-T	110°12'26.18"	39°43'53.15"	0.2 cm	GXG	#5-1
DS6-1-T	110°23'5.52"	39°48'25.92"	1 cm	CNL	#6-1
DS6-2s-T	110°24'19.44"	39°39'44.45"	3 cm	LJL	#6-2s
DS6-2z-T	110°18'31.67"	39°47'48.15"	2 cm	NY	#6-2z
DS7-T	110°23'5.52"	39°48'25.92"	7 cm	CNL	#7

Formation in the Dongsheng Coalfield were formed during the Aalenian Stage of the Middle Jurassic (Zhang et al., 2020, 2021).

3. Samples and analytical procedures

3.1. Sample collection

In this study, five open-pit mines in the Dongsheng Coalfield, including the Nangai (NG), Gaoxigou (GXG), Lijialiang (LJL), Chan-naoliang (CNL), and Nayuan (NY) sites (Fig. 1B), were chosen for sample collection. All tonsteins within the coal seams in the coal mines have distinctive features, such as gray to white color, persistent lateral extent, sharp contacts with adjacent coals, and thin thicknesses varying between 0.2 and 7 cm (Fig. 2 and Table 1). To determine the nature of the tonsteins and the mobility of its trace elements leaching into enclosing coals, both tonsteins and coal benches underlying and overlying the tonsteins were collected. All sample were named with a letter of T, U, and O for tonsteins, underlying coal and overlying coal, respectively. A total of six tonsteins samples were collected from NG (DS3-1-T within 60-cm-thick coal bed, 4-m above coal seam #3-1), GXG (DS5-1-T within coal seam #5-1), CNL (DS6-1-T within coal seam #6-1 and DS7-T within coal seam #7), LJL (DS6-2s-T within coal seam #6-2s) and NY (DS6-2z-T within coal seam #6-2z) coal mines (Fig. 1C). The sampling width of the adjoining coals is 30 cm above and below the tonsteins with a 10-cm interval for each sample. Note that only one overlying coal sample for DS5-1-T was collected due to 12 cm of length between roof strata and #5-1 coal seam. Thus, a total of 34 samples of tonstein-bearing coals were collected in detail in the five coal mines (Fig. 2). After collection, all samples were directly packed into plastic bags to avoid weathering and contamination. Details on the samples collected are shown in Table 1. In addition, DS5-1-T intercalated coal seam #5-1 in the GXG coal mine was collected for zircon U—Pb dating.

3.2. Analytical procedures

In order to analyze for mineralogical characteristics and compositions of the six tonsteins samples, polished thin-sections were examined using an optical microscope (Leica DFC550). Further analysis of the minerals was carried out by X-ray powder diffraction (XRD) using a PANalytical X'Pert Pro model instrument at the Micro Structure Analytical Laboratory in Peking University Science Park. The samples were powdered using a tungsten carbide mill, then prepared as back-filled mounts to scan from 5 to 70° 2θ with 0.02° steps. For comprehensive identification of the clay minerals, the clay (< 2 μm) fractions of the samples were separated by ultrasonic dispersion in water with sodium hexametaphosphate (Calgon) and by subsequent settling for 2 h. The clay fractions were placed evenly on glass slides and then scanned in an air-dried state, then after saturation with glycol overnight and after heat treatment at 450°C for 2.5 h. Quantitative mineralogical analyses were performed by the software Siroquant™ (Taylor, 1991) based on the obtained XRD patterns. Further details of this technique are given by Dai et al. (2018).

Table 2
Quantitative mineral contents of six tonsteins.

Sample	Kaolinite (%)	Quartz (%)	Chlorite (%)	Smectite (%)
DS3-1-T	73	9		18
DS5-1-T	100			
DS6-1-T	96	3		1
DS6-2s-T	94	2	4	
DS6-2z-T	94	2	4	
DS7-T	98	2		

The modes and composition of occurrence of finely dispersed minerals of the six tonsteins samples were carried out using two scanning electron microscopes (SEM, Phenom prox and Nova Nano SEM450) combined with an energy-dispersive X-ray spectrometer (EDS) in the Shandong Provincial Key Laboratory of Depositional Mineralization and Sedimentary Minerals, Shandong University of Science and Technology. Before the examination, specimens were coated with a conductive layer of platinum.

Prior to analysis for major element oxides (SiO_2 , TiO_2 , Al_2O_3 , Fe_2O_3 , MnO , MgO , CaO , Na_2O , K_2O , and P_2O_5), the powdered tonsteins samples were ashed at a temperature of 960°C for 2.5 h in an inductive oven and the residues were measured on an elemental analysis by wavelength dispersive X-ray fluorescence spectrometer (XRF-1800). Trace elements in the tonsteins were determined using an inductively coupled plasma mass spectrometer (ICP-MS, Agilent 7500a). The powdered samples were dissolved in a mixture of concentrated nitric, hydrofluoric, and hydrochloric acids, and then subjected to a further nitric acid digestion following the approach reported by Dai et al. (2011). The elemental analyses of the tonstein samples were completed in the Lab. Center, Institute of Earth Sciences, China University of Geosciences (Beijing).

For all 34 enclosing coal samples, trace elements contents were determined using a high resolution inductively coupled plasma mass spectrometer (HR-ICP-MS, Element XR) in the Analytical Laboratory Beijing Research Institute of Uranium Geology following the procedure as outlined by Wang et al. (2018). The samples were crushed and ground to less than 200 mesh, and then subjected to digestion using mixed acid reagents consisting of 1.5 ml HNO_3 and 1.5 ml HF in oven at 190°C for 48 h. The solution was at ~140°C to dryness followed by adding 1 ml HNO_3 and evaporating to the second round of dryness, and then redissolved by ~3 ml of 30% HNO_3 and resealed and heated in the bomb at ~190°C for 12–24 h. The final solution was diluted to about 100 g with mixture of 2% HNO_3 for ICP-MS analysis.

For the DS5-1-T sample, zircon grains were extracted concentrated through heavy-liquid techniques and then hand-picked using a stereomicroscope. The extracted grains were mounted in resin and polished until the center of the embedded grains was exposed on the surface. Then, the zircon grain were examined using cathodoluminescence (CL) images for morphology analysis. After imaging, the selected zircon grains were subjected to U—Pb dating using Laser ablation-inductively coupled plasma-mass spectrometry (LA-ICP-MS) at the State Key Laboratory of Geological Processes and Mineral Resources, China University of Geosciences, (Beijing).

4. Results

4.1. Mineralogical compositions

As the XRD result shown, apart from Sample DS3-1-T, the tonsteins are composed of kaolinite (94%–100%) and quartz (0%–3%), with small amounts of smectite (0%–1%) and chlorite (0%–4%) (Table 2). Sample DS3-1-T has the lowest kaolinite (73%) and highest quartz (9%) and smectite (18%) contents. Some kaolinites are found as a well-ordered crystal structure occurring as vermicular aggregates (Fig. 3A–C), which are considered evidence of a volcanic origin (Dai et al., 2017; Ruppert and Moore, 1993; Spears, 2012; Hower et al., 2018). Moreover,

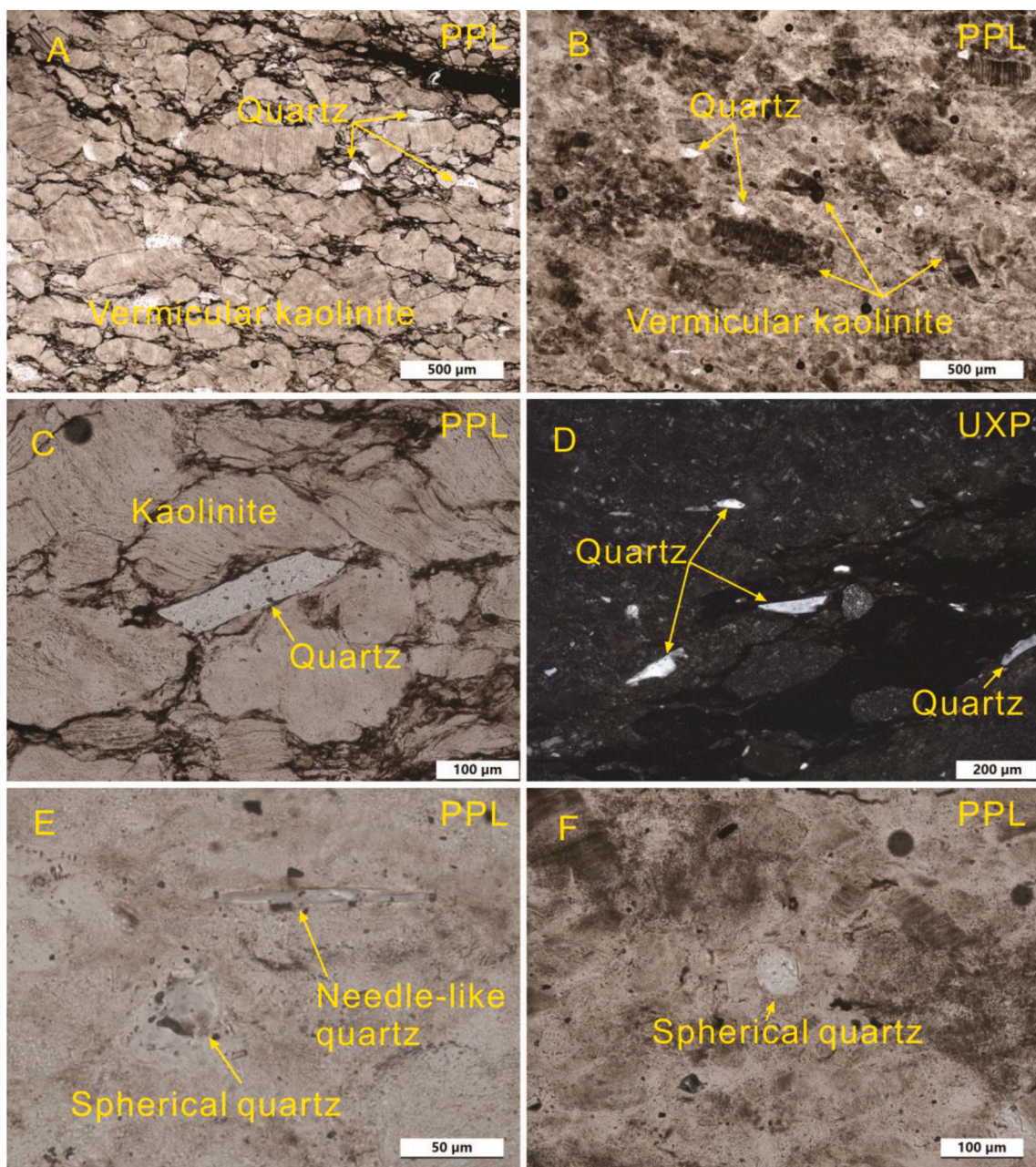


Fig. 3. Petrographic composition of the tonsteins. (A) vermicular kaolinite and angular quartz of DS6-2z-T, PPL (plane polarized light under optical microscope). (B) vermicular kaolinite and angular quartz in kaolinite matrix of DS3-1-T, PPL. (C) Well-ordered kaolinite and angular quartz of DS6-2z-T, PPL. (D) Angular quartz fragments of DS6-2s-T, UXP (crossed polarized light under microscope). (E) Spherical and needle-like quartz of DS7-T, PPL. (F) Spherical quartz in kaolinite matrix of DS6-1-T, PPL.

the kaolinite occurs as a cryptocrystalline matrix surrounding other discrete particles, such as vermicular kaolinite (Fig. 3B) and quartz (Fig. 3E and F). The quartz fragments show angular (Fig. 3A–D) and needle-like (Fig. 3E) shapes, which is associated with pyroclastic origin rather than normal sedimentary processes (Arbuzov et al., 2016; Dai et al., 2017; Shen et al., 2021). However, minor spherical quartz observed in sample DS3-1-T indicates a detrital origin (Fig. 3F) and may be cause of an increase in quartz content in this tonstein.

In addition to the minerals detected by XRD analysis, biotite (Fig. 4A and B), muscovite (Fig. 4C and D), and apatite (Fig. 4E and F) were only identified using optical microscopy due to their low abundances. Some biotite was subjected to chloritization with a sheaf- or broom-like form (Fig. 4A and B) causing lesser chlorite in the XRD scans of DS6-2s-T and DS6-2z-T (Table 1). The occurrence of biotite may provide evidence of

volcanic ash (Bouroz, 1967; Dai et al., 2017). The muscovite is usually a terrigenous detrital material (Bohor and Triplehorn, 1993; Dai et al., 2017), consistent with the observed spherical quartz indicating a detrital origin in DS3-1-T. The apatite can usually be indicative of volcanic input (Dai et al., 2017; Hower et al., 1999, 2016; Mardon and Hower, 2004; Zhao et al., 2012) occurring as elongate grains (Fig. 4E and F). In some cases, the delicate apatite grains have been fractured due to compaction (Fig. 4E) (Spears, 2012).

Using SEM and EDS techniques, pyrite (Fig. 5A–C and F) and other sulfides, such as barite (Fig. 5D and E), sphalerite (Fig. 5F and G), and galena (Fig. 5H and I), which are thought to be generally epigenetic (Arbuzov et al., 2016), were determined in tonsteins. As a resistant accessory mineral, euhedral crystals of zircon with well-developed crystal faces were mostly present in the tonstein samples (Fig. 6A, B,

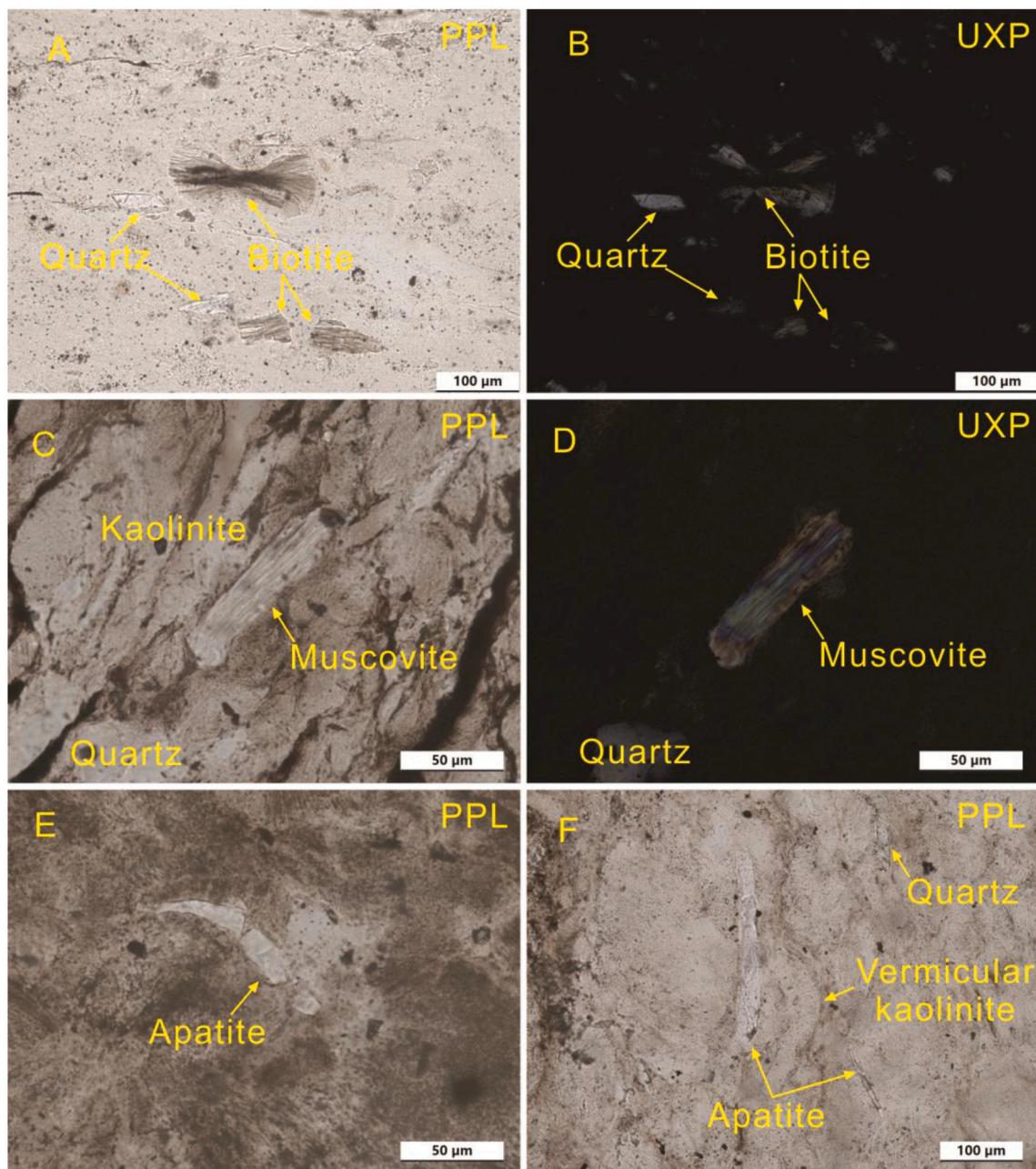


Fig. 4. Petrographic composition of the tonsteins. (A-B) Sheaf-shape biotite and angular quartz of DS3-1-T, PPL and UXP. (C-D) Pseudomorph of muscovite in DS6-1T, PPL and UXP. (E) Fractured apatite of DS3-1-T, PPL. (F) elongate apatite, vermicular kaolinite, and angular quartz in kaolinite matrix of DS6-1-T, PPL.

and G). In addition, some detrital zircons surrounded by cryptocrystalline kaolinite were observed in the tonsteins (Fig. 6C–E, H, and I) (Zhang et al., 2021). Common euhedral zircon grains in tonstein are not only an indicator of pyroclastic origin (Dai et al., 2014a; Dai et al., 2017), but may suggest that the original ash composition was possibly felsic (Arbusov et al., 2016). However, Sutherland et al. (2016) found that zircon crystals are also abundant in alkaline rocks. Due to a low abundance and susceptibility to alteration, sanidine is only observed in DS6-2z-T (Fig. 6F and J).

Radiometric dating of volcanogenic zircons in tonstein produces near-concordant ages (Bohor and Triplehorn, 1993; Spears, 2012; Nechaev et al., 2021). Zhang et al. (2021) have used radiometric age determinations on zircons in five tonsteins (corresponding to the samples of DS3-1-T, DS6-1-T, DS6-2s-T, DS6-2z-T, and DS7-T) to determine the absolute ages of the Yan'an Formation in the Ordos Basin, which

indicates the tonsteins are altered volcanic ash falls. In this study, 10 zircon grains from sample DS5-1-T were selected for dating using LA-ICP-MS. Cathodoluminescence (CL) images suggest that the zircons have an excellent euhedral morphology with length to width ratios >2 and clear oscillatory zoning, indicating a magmatic origin (Fig. 7A). The zircon grains of DS5-1-T show similar $^{206}\text{Pb}/^{238}\text{U}$ ages ranging from 172 ± 1 Ma to 175 ± 2 Ma (Table 3), with a weighted mean age of 173.07 ± 0.53 Ma (MSWD = 1.5, N = 10) (Fig. 7), which is an agreement with the chronostratigraphic framework for the Yan'an Formation of the Ordos Basin (Zhang et al., 2021). Similar to the other five tonsteins, the DS5-1-T also originates from the alteration of volcanic ash based on significant evidence of the concordant zircon ages.

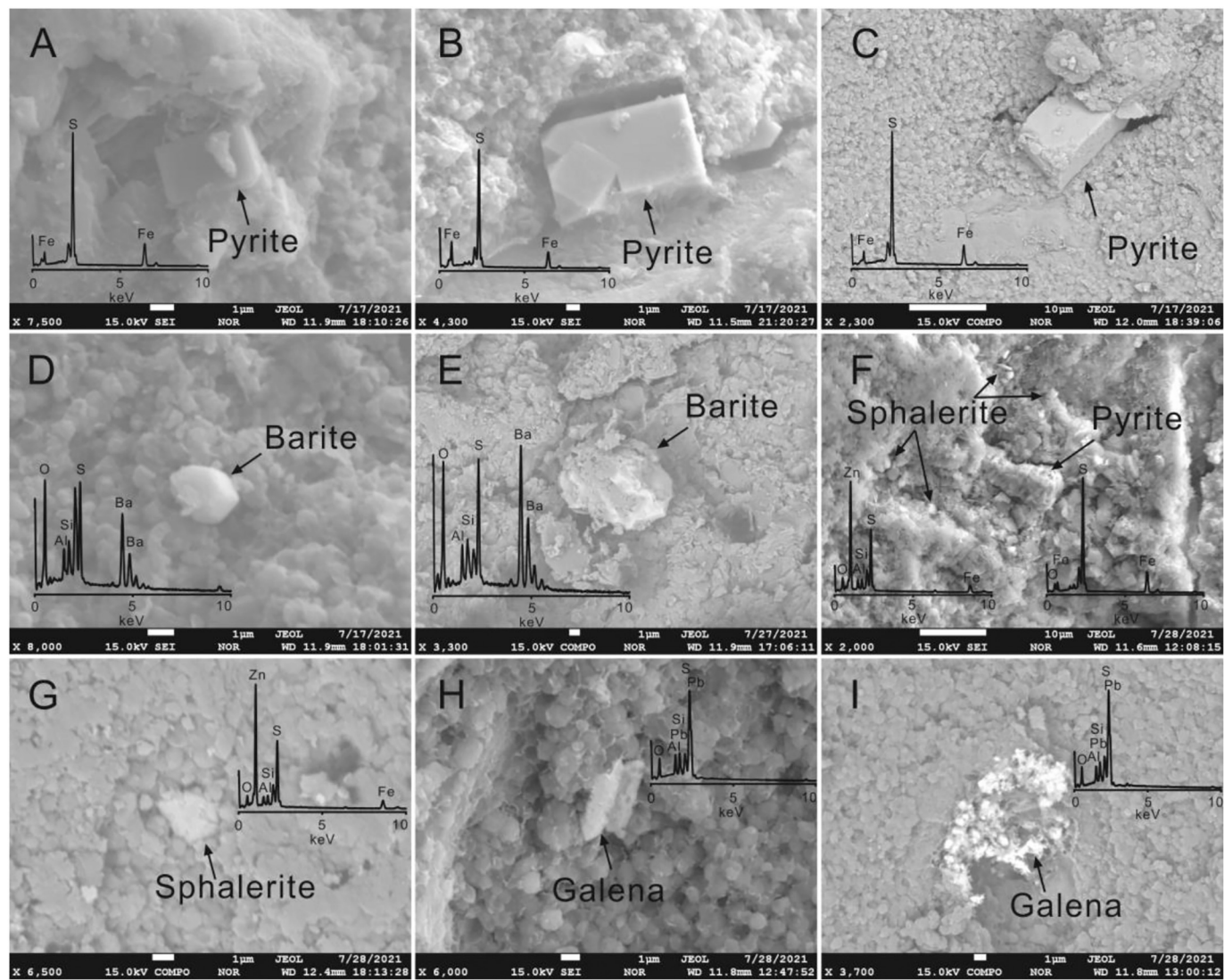


Fig. 5. (A-B) SEM secondary electron images and EDS spectra of pyrite in DS3-1-T. (C) SEM back-scattered electron image and EDS spectrum of pyrite in DS6-1-T. (D) SEM secondary electron image and EDS spectrum of barite in DS6-2s-T. (E) SEM back-scattered electron image and EDS spectrum of barite in DS6-2s-T. (F) SEM secondary electron image and EDS spectra of barite and pyrite in DS6-2z-T. (G) SEM back-scattered electron image and EDS spectrum of barite in DS7-T. (H) SEM secondary electron image and EDS spectrum of galena in DS3-1-T. (I) SEM back-scattered electron image and EDS spectrum of galena in DS6-1-T.

4.2. Geochemical compositions

4.2.1. Major elements

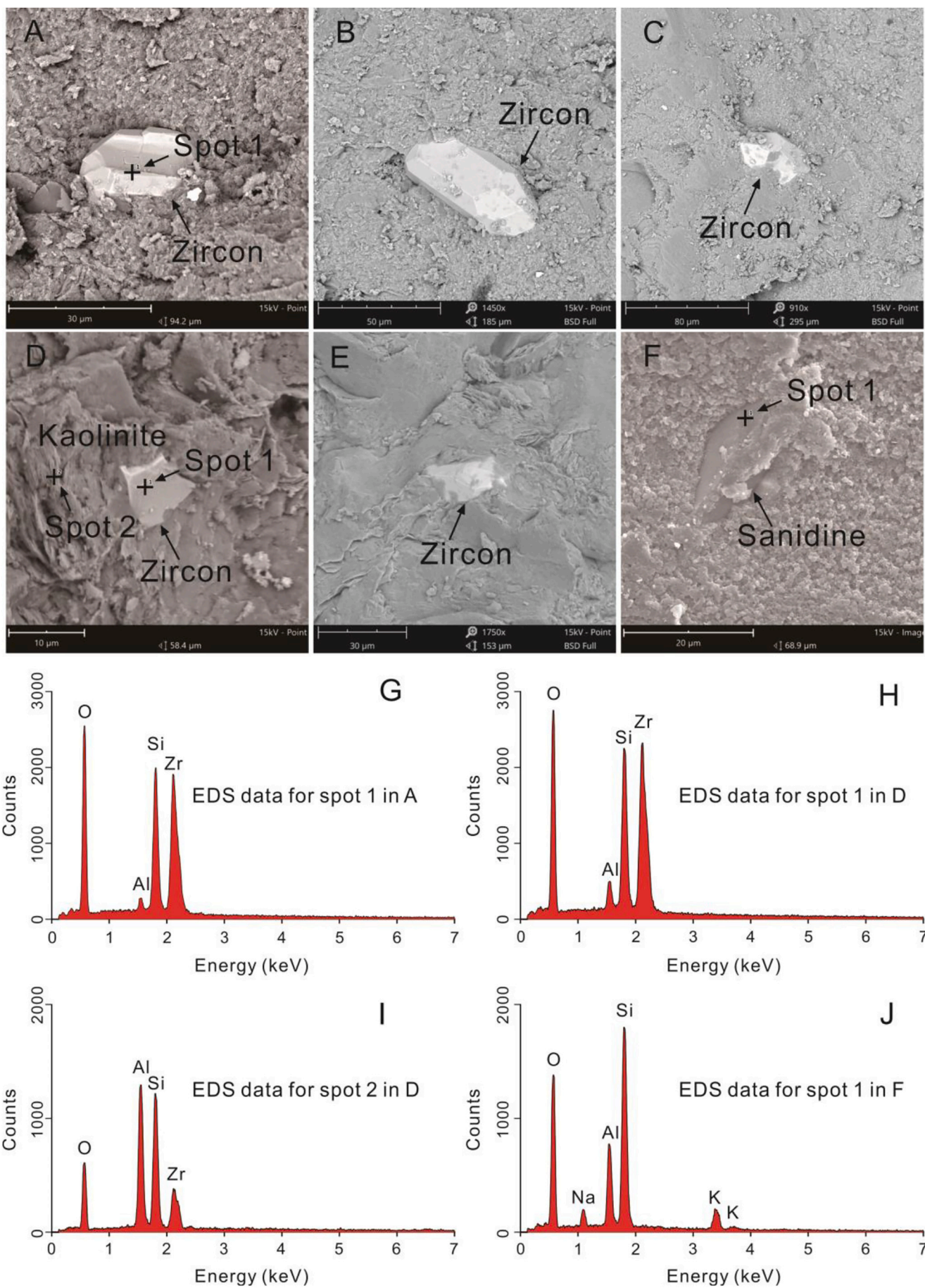
The results of whole-rock major element analyses of six tonstein samples are given in Table 4. LOI values are high and widely range from 15.08 to 38.8% due to the high content of organic matter in the tonsteins (Fig. 2F). In comparison with the clay shale (Grigor'ev, 2003), the tonsteins contain high Al_2O_3 (23.64–36.01%) and SiO_2 (34.16–57.75%); low TiO_2 (0.19–0.59%), Fe_2O_3 (0.16–1.68%), MgO (0.11–1.10%), CaO (0.21–2.31%), Na_2O (0.01–0.19%), and K_2O (0.04–0.26%); and negligible MnO (< 0.01%) and P_2O_5 (< 0.03%) (Fig. 8). $\text{SiO}_2/\text{Al}_2\text{O}_3$ ratios of the tonstein samples ranging from 1.24 to 2.44 are slightly higher than an idealized kaolinite $\text{SiO}_2/\text{Al}_2\text{O}_3$ value (1.18) due to the small amount of quartz and sanidine in the tonsteins as mentioned above.

4.2.2. Trace elements and rare earth elements and yttrium (REY)

The contents of trace elements and REY in the tonsteins and enclosing coals are shown in Tables 5 and 6. Compared to the mean composition of clay shale (Grigor'ev, 2003), all tonstein samples present similar trace element abundances, which are substantially enriched in Ga, W, Pb, Bi, Th, U, Nb, Ta, and Hf and depleted in Be, Sc, V, Cr, Co, Ni,

Cu, Zn, Rb, Sr, Cd, Sb, Cs, Tl, Zr, and REY (Fig. 9). Apart from the tonstein sample DS3-1-T, the enclosing coals of the remaining tonstein samples (DS5-1-T, DS6-1-T, DS6-2s-T, DS6-2z-T, DS7-T) have a comparable enrichment characteristic of the trace elements with elevated concentrations in Sr, Th, U, Nb, Ta, Zr, and Hf, compared with the values for world hard coals (Ketris and Yudovich, 2009) (Fig. 10). However, more trace elements are enriched in the enclosing coals of DS3-1-T, including Be, Sc, V, Cr, Co, Ni, Cu, W, and REY (Fig. 10), especially the concentration coefficient (CC = ratios of element concentration in investigated coals vs. world hard coals, Dai et al., 2015) of Co reached an abnormal 23.8 due to high concentrations of Co (>175 ppm) in enclosing coal samples (DS3-1-U1, DS3-1-O1, DS3-1-O2, and DS3-1-O3) (Table 4). This high Co concentration level may be associated with organic matter, sulfides, and aluminosilicates because a high degree of uncertainty of modes of occurrence of Co (Finkelman, 1994; Dai et al., 2021).

Rare earth elements and yttrium (REY) have been extensively used as geochemical indicators for the altered volcanic ashes within coal-bearing strata (Arbusov et al., 2016; Dai et al., 2011, 2014a; Dai et al., 2017; Hower et al., 1999; Zhou et al., 2000) due to their coherent behavior during different geochemical processes and their predictable



(caption on next page)

Fig. 6. (A) SEM back-scattered electron image of euhedral zircon in DS3-1-T. (B) SEM back-scattered electron image of euhedral elongate zircon in DS6-1-T. (C) SEM back-scattered electron image of euhedral zircon in DS6-2s-T. (D) SEM back-scattered electron image of euhedral zircon in DS6-2z-T. (E) SEM back-scattered electron image of euhedral zircon in DS7-T. (F) SEM back-scattered electron image of sanidine in DS6-2z-T. (G) EDS data for spot 1 in (A) of DS3-1-T. (H) EDS data for spot 1 in (D) of DS6-2z-T. (I) EDS data for spot 2 in (D) of DS6-2z-T. (J) EDS data for spot 1 in (F) of DS6-2z-T.

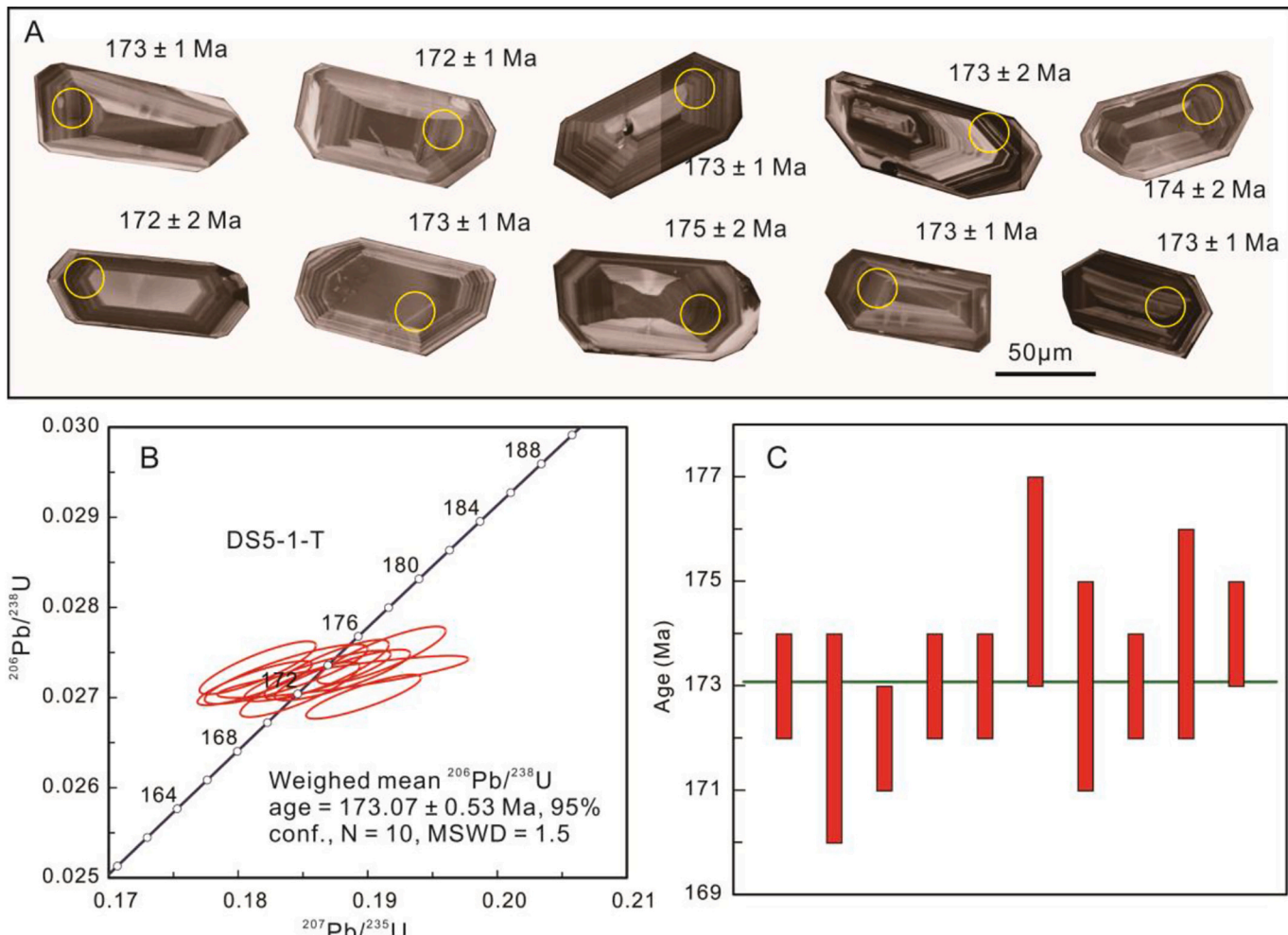


Fig. 7. (A) Cathodoluminescence (CL) images showing the internal structure for zircons of tonstein DS5-1-T. The analytical spots for U—Pb (small yellow circles) and ages (in Ma) are shown. (B) U—Pb concordia plots for DS5-1-T. Weighted mean age are shown. (C) Weighted mean age diagram for zircons in DS5-1-T. Vertical bars represent the $^{206}\text{Pb}/^{238}\text{U}$ date and 2σ analytical uncertainty of individual analyses. (For interpretation of the references to color in this figure legend, the reader is referred to the web version of this article.)

patterns of fractionation (Bau et al., 2014; Dai et al., 2017; Spears, 2012). According to the classification of Seredin and Dai (2012), a three-fold partition of REY are classified as light (LREY: La, Ce, Pr, Nd, and Sm), medium (MREY: Eu, Gd, Tb, Dy, and Y), and heavy (HREY: Ho, Er, Tm, Yb, and Lu). In general, REY concentrations in tonsteins can be normalized to both chondrite (Arbusov et al., 2016; Dai et al., 2011; Hower et al., 1999; Zhou et al., 2000) and classic sedimentary rocks (e.g., UCC, Upper Continental Crust) (Dai et al., 2014a; Shen et al., 2021), because tonsteins in coal-bearing sequences have a combination of igneous origin and subsequent sedimentary processes (Dai et al., 2017). Compared with chondrite-normalized REY distribution patterns for in tonsteins, UCC-normalized REY distribution patterns can not only indicate the original magmatic sources but also evaluate changes during the diagenetic and epigenetic stages of development (Dai et al., 2017; Shen et al., 2021), with three enrichment types of L-type ($\text{La}_N/\text{Lu}_N > 1$), M-type ($\text{La}_N/\text{Sm}_N < 1$, $\text{Gd}_N/\text{Lu}_N > 1$), and H-type ($\text{La}_N/\text{Lu}_N < 1$) (Seredin and Dai, 2012).

The concentrations of total REY in the tonstein samples range from

24.90 ppm at DS6-2s-T to 110.75 ppm at DS6-1-T with an average of 70.55 ppm (Table 4). On the chondrite-normalized (Taylor and McLennan, 1985) REY patterns, all the tonsteins have a similar subparallel trend of REY distribution characterized by high elevated LREY concentrations with significant negative Eu anomalies (expressed as $\text{Eu}_N/\text{Eu}_N^* = \text{Eu}_N / [(\text{Sm}_N \times 0.67) (\text{Tb}_N \times 0.33)]$, Dai et al., 2016), ranging from 0.28 to 0.54 (Fig. 11A). Apart from the samples DS5-1-T and DS6-2s-T, the UCC-normalized (Taylor and McLennan, 1985) REY patterns of the other four tonsteins also show L-type enrichment, strong negative Eu anomalies ($\text{Eu}_N/\text{Eu}_N^*$ values from 0.56 to 0.85), and slight negative Y anomalies ($\text{Y}_N/\text{Ho}_N = 0.85\text{--}0.96$) (Fig. 11B). In contrast, the samples DS5-1-T and DS6-2s-T have a distinctly H-type enrichment with negative Eu anomalies of 0.81 and 0.43, and a negative Y anomaly ($\text{Y}_N/\text{Ho}_N = 0.83$) for the tonstein DS6-2s-T (Fig. 11B).

Table 3

Zircon LA-ICP-MS U—Pb analytical data of the tonstein DS5-1-T.

Spot	Isotopic ratios					
	$^{207}\text{Pb}/^{206}\text{Pb}$	1 σ	$^{207}\text{Pb}/^{235}\text{U}$	1 σ	$^{206}\text{Pb}/^{238}\text{U}$	1 σ
DS5-1-T-01	0.04932	0.00122	0.18612	0.00463	0.02724	0.00023
DS5-1-T-02	0.04931	0.00103	0.18477	0.00377	0.02709	0.00025
DS5-1-T-03	0.05083	0.00101	0.18967	0.00362	0.02701	0.0002
DS5-1-T-04	0.04995	0.00204	0.18809	0.00793	0.02723	0.00019
DS5-1-T-05	0.04997	0.00113	0.18805	0.00428	0.02725	0.00023
DS5-1-T-06	0.05026	0.00096	0.19106	0.00406	0.02747	0.00026
DS5-1-T-07	0.04891	0.00142	0.18371	0.00515	0.02726	0.00027
DS5-1-T-08	0.04829	0.00094	0.18128	0.00362	0.02716	0.0002
DS5-1-T-09	0.04981	0.00118	0.18683	0.00393	0.02731	0.00027
DS5-1-T-10	0.04822	0.00105	0.18151	0.00368	0.02733	0.00024
Spot	Age (Ma)					
DS5-1-T-01	$^{207}\text{Pb}/^{206}\text{Pb}$	1 σ	$^{207}\text{Pb}/^{235}\text{U}$	1 σ	$^{206}\text{Pb}/^{238}\text{U}$	1 σ
DS5-1-T-02	163	42	173	4	173	1
DS5-1-T-03	162	31	172	3	172	2
DS5-1-T-04	233	30	176	3	172	1
DS5-1-T-05	193	85	175	7	173	1
DS5-1-T-06	194	37	175	4	173	1
DS5-1-T-07	207	32	178	3	175	2
DS5-1-T-08	144	47	171	4	173	2
DS5-1-T-09	113	33	169	3	173	1
DS5-1-T-10	186	31	174	3	174	2
	110	32	169	3	174	1

Table 4

Major element concentrations on whole-rock basis (%) in tonsteins.

Sample	DS3-1-T	DS5-1-T	DS6-1-T	DS6-2s-T	DS6-2z-T	DS7-T	Mean	Clay shale*
SiO ₂	57.75	34.16	46.40	43.81	44.56	53.29	46.66	50.30
TiO ₂	0.22	0.19	0.45	0.59	0.56	0.37	0.40	0.50
Al ₂ O ₃	23.64	24.13	36.01	35.43	35.84	27.18	30.37	16.60
Fe ₂ O ₃	1.27	1.68	0.35	0.51	0.27	0.16	0.71	6.70
MnO	0.001	0.004	0.005	0.008	0.004	0.001	0.004	0.120
MgO	0.55	0.26	0.25	0.17	0.11	1.10	0.41	2.75
CaO	0.49	0.57	0.29	0.25	0.21	2.31	0.69	3.10
Na ₂ O	0.07	0.04	0.01	0.19	0.01	0.04	0.06	1.38
K ₂ O	0.26	0.12	0.06	0.12	0.06	0.04	0.11	3.28
P ₂ O ₅	0.01	0.03	0.02	0.03	0.03	0.00	0.02	0.18
LOI	15.42	38.80	15.89	18.62	17.93	15.08	20.29	–
SiO ₂ / Al ₂ O ₃	2.44	1.42	1.29	1.24	1.24	1.96	1.54	3.03
Al ₂ O ₃ / TiO ₂	107.45	127.00	80.02	60.05	64.00	73.46	75.93	33.20

Note: * Grigor'ev (2003).

5. Discussion

5.1. Evidence for volcanic origin

The field characteristics and mineralogical compositions can provide evidence for volcanic origin for tonsteins (Dai et al., 2017 and references therein). Similar in macroscopically typical features to altered volcanic ash in coal-bearing sequences (e.g., Arbusov et al., 2016; Dai et al., 2014a; Shen et al., 2021), six tonsteins of the Yan'an Formation in the field are found as thin beds with a pale color, lateral continuity, conchoidal and flint-like fracture planes, sharp contacts with enclosing coals, and an absence of sedimentary layering structure (Fig. 2). The presence of volcanogenic minerals, such as high-temperature quartz, sanidine, micas, zircon, and apatite in the intra-seam clay beds may indicate an ash fall origin (Bouroz, 1967; Dai et al., 2017; Spears, 2012; Ward, 2002). Moreover, the quartz in altered volcanic ashes has an angular habit in shape and common splinters, which form far from normal sedimentary mudrocks (Spears, 2012). In the present study, the tonstein samples have vermicular kaolinites (Fig. 3A–C) and irregular quartz grains (Fig. 3A–D), and many euhedral zircon crystals (Fig. 6A–E) with similar U—Pb ages (Fig. 7) (Zhang et al., 2020; Zhang et al., 2021), indicating that the tonsteins were formed during a very short time

interval. All of the above lines of evidence suggest that the six tonsteins in the Yan'an Formation of the Ordos Basin are altered volcanic ashes. However, the rounded quartz, muscovite, and detrital zircons are also observed in the samples, indicating that a small amount of terrigenous debris from the nearby orogenic belts have some contribution to the tonsteins.

5.2. Identification of original magma source

The three groups of tonsteins have been referred to as felsic, intermediate (or alkaline), and mafic tonsteins, indicating their original magmas (Dai et al., 2011, 2017; Spears, 2012; Zhou et al., 2000). Some of the euhedral pyroclastic minerals in tonsteins can interpret the original magmatic composition, such as sanidine and zircon (Arbusov et al., 2016; Zhao et al., 2012). For example, Zhao et al. (2012) suggested that sanidine crystals in two tonsteins intercalated with the Great Northern coal seam of the Sydney Basin in Australia may represent members of the anorthoclase–sanidine series or sodic sanidine and indicate a felsic to intermediate volcanic ash. The presence of sanidine in the tonstein DS6-2z-T shows that the original ash composition was also possibly felsic to intermediate (Fig. 6F).

The geochemistry of altered volcanic ashes is more appropriate for

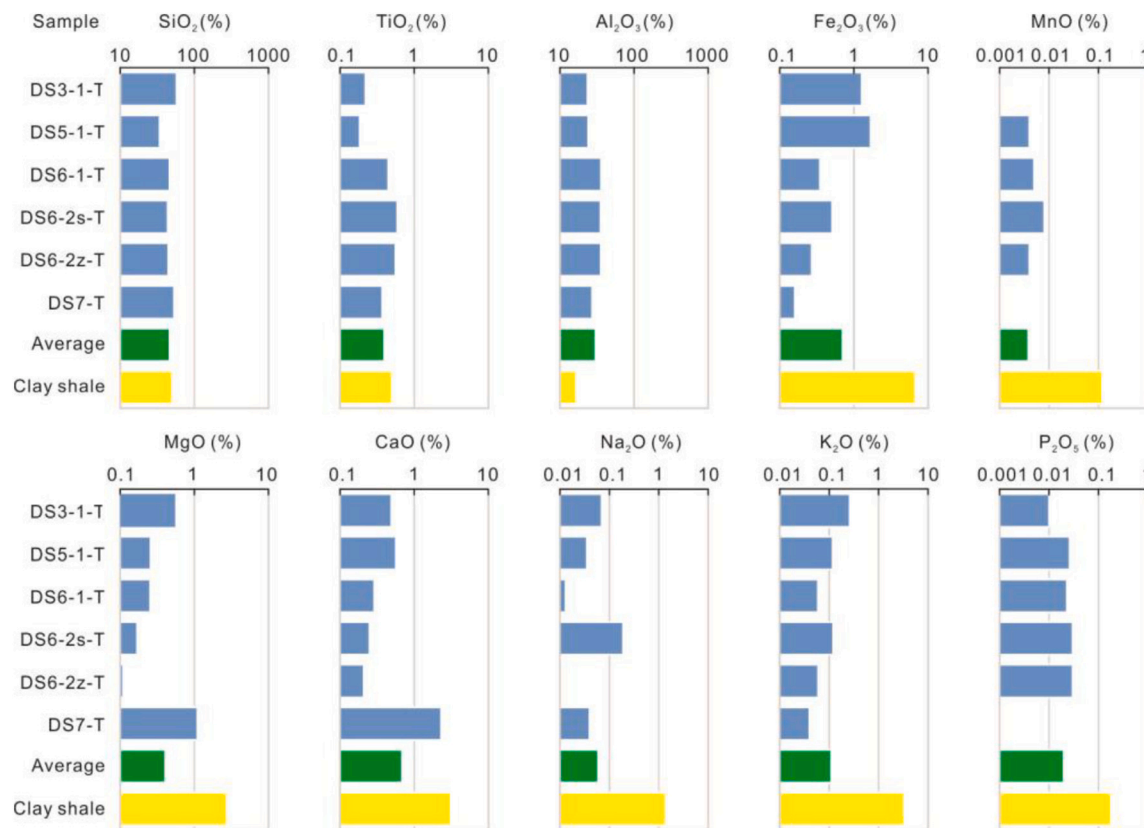


Fig. 8. Major elements in tonsteins and clay shale (Grigor'ev, 2003).

volcanic ash classification (Spears, 2012; Dai et al., 2017). Generally, some elements, including Al, Ti, Zr, Hf, Y, Nb, Ta, and rare earth elements, have distinct concentrations in different magmas and are mostly used to constrain the original igneous sources of volcanic ashes due to their relative immobility (Hayashi et al., 1997; Wesolowski, 1992; Zielinski, 1985; Ziemiak et al., 1993). The $\text{Al}_2\text{O}_3/\text{TiO}_2$ ratio is commonly used for the classification of altered volcanic ashes (e.g., Anggara et al., 2018; Dai et al., 2011, 2014a; Shen et al., 2021; Spears and Kanaris-Sotiriou, 1979; Wang et al., 2020; Zhao et al., 2012). Typical $\text{Al}_2\text{O}_3/\text{TiO}_2$ values for corresponding felsic, intermediate, and mafic tonsteins are >50, 12.5–50, and <12.5, respectively (Dai et al., 2011, 2014a, 2017; Spears and Kanaris-Sotiriou, 1979; Winchester and Floyd, 1977). For this study, the $\text{Al}_2\text{O}_3/\text{TiO}_2$ ratios of the studied samples range from 64.00 at DS6-1-T to 130.43 at DS7-T (Fig. 11C), suggesting that the tonsteins in the Yan'an Formation were initially sourced from felsic rocks.

In addition to $\text{Al}_2\text{O}_3/\text{TiO}_2$, the Zr/TiO_2 versus Nb/Y plot of Winchester and Floyd (1977) has also been widely used to deduce the origin of altered volcanic ashes (e.g., Dai et al., 2011; Spears, 2012; Arbuzov et al., 2016; Spears and Arbuzov, 2019; Wang et al., 2020), which can classify tonsteins using the volcanic nomenclature, such as rhyolitic tonstein. However, in the Zr/TiO_2 - Nb/Y diagram, the tonstein samples plot within the rhyodacite-dacite (DS5-1-T), trachyte (DS3-1-T and DS6-2z-T), and basanite-nephelinite (DS6-1-T, DS6-2s-T and DS7-T) fields rather than the rhyolite field (Fig. 11D). This distribution may be due to the loss of Y concentration in the tonsteins because Y can be mobile in the peat-forming environment (Dai et al., 2016, 2017; Möller, 2000; Wang et al., 2020), which is supported by negative anomalies of Y in the tonstein samples (Fig. 11B). Hence, the classification diagram of Winchester and Floyd (1977) could be less reliable as a provenance indicator for the tonsteins in this study. In such a case, the diagrams of Zr/TiO_2 - $\text{Al}_2\text{O}_3/\text{TiO}_2$ and Nb/Yb - $\text{Al}_2\text{O}_3/\text{TiO}_2$ were used to discriminate between volcaniclastic deposits of different origins (Shen et al., 2021;

Zheng et al., 2020). The U–Pb ages of the zircon grains in the tonsteins of the Yan'an Formation (Zhang et al., 2020, 2021 and this study) constrain that the original volcanic eruption occurred in the Aalenian Stage of the Middle Jurassic. Due to a small amount of geochemical data of Aalenian pyroclastic rocks in the North China craton, we have used the Mesozoic volcanic rocks to identify the original igneous sources in the plotting Zr/TiO_2 - $\text{Al}_2\text{O}_3/\text{TiO}_2$ and Nb/Yb - $\text{Al}_2\text{O}_3/\text{TiO}_2$ diagrams. As shown in Fig. 12, all plots of six tonstein samples are situated in or near the rhyolite field, which is consistent with a felsic composition for the initial material of the tonsteins as deduced earlier. It is noteworthy that elements Zr and Nb in the peat-forming environment could be relatively mobile (Dai et al., 2017 and references therein; Spears and Arbuzov, 2019). Indeed, Zr and Nb in the tonsteins of the Yan'an Formation have been leached into their enclosing coals (detail are discussed below). Therefore, combinations of the Zr/TiO_2 - $\text{Al}_2\text{O}_3/\text{TiO}_2$ and Nb/Yb - $\text{Al}_2\text{O}_3/\text{TiO}_2$ diagrams with other geochemical indicators for provenance analysis would be more appropriate (Dai et al., 2017).

Another geochemical feature indicating a possible original magmatic material of the tonsteins is the REY concentrations and distribution patterns (e.g., Arbuzov et al., 2016; Wang et al., 2020; Dai et al., 2017; Shen et al., 2021). In this study, the six tonstein samples characteristically have low REY concentrations and pronounced negative Eu anomalies with a distinctive fractionation between LREY and HREY, indicating a typical felsic source. Thus, overall, all the tonsteins in the Yan'an Formation of the Ordos Basin have a felsic (rhyolite) composition of the initial volcanogenic material.

It may be mentioned that the occurrence and abundance of smectite are commonly observed in altered volcanic ashes of intermediate and mafic compositions (Bohor and Triplehorn, 1993; Reinink-Smith, 1990; Spears, 2012; Triplehorn et al., 1977; Turner et al., 1983) or thick layers (Bohor and Triplehorn, 1993; Bouroz et al., 1983; Triplehorn and Bohor, 1981; Zaritsky, 1985). In this study, the tonstein within the coal layer above coal seam #3-1 is thin, 1.3-cm thick (Fig. 2A), and has a parent

Table 5

Trace element concentrations on ash basis (ppm) in tonsteins and enclosing coals.

Sample	Li	Be	Sc	V	Cr	Co	Ni	Cu	Zn	Ga	Rb	Sr	Mo	Cd
DS3-1-O3	3.3	8.2	9.9	237.0	58.9	179.0	64.1	37.6	22.6	13.0	10.6	151.0	1.0	0.02
DS3-1-O2	7.2	5.3	6.5	17.7	13.8	177.0	45.9	33.3	22.1	11.4	11.6	137.0	1.1	0.07
DS3-1-O1	6.4	4.9	5.6	13.3	11.6	221.0	48.0	35.5	24.7	8.7	7.2	138.0	1.1	0.07
DS3-1-T	84.2	0.9	5.6	3.2	2.0	2.9	11.3	4.9	23.0	28.2	10.2	123.0	0.3	0.14
DS3-1-U1	4.1	4.2	3.4	89.4	23.3	207.0	53.2	32.5	21.0	5.3	3.9	150.0	1.5	0.10
DS3-1-U2	7.3	4.9	3.4	46.0	21.0	65.1	23.7	34.4	24.7	5.2	7.6	141.0	1.1	0.03
DS3-1-U3	0.5	8.4	2.1	92.3	16.7	6.2	9.0	20.6	17.4	2.1	0.4	243.0	0.8	0.04
DS5-1-O1	0.9	6.7	8.5	25.3	22.1	5.2	4.8	5.2	6.0	2.9	0.8	463.0	0.3	0.02
DS5-1-T	10.4	2.8	4.2	11.1	10.2	13.1	14.3	4.8	9.8	29.3	4.2	176.0	0.7	0.06
DS5-1-U1	3.2	4.5	5.9	8.5	9.4	6.0	5.5	3.1	7.7	8.9	1.0	429.0	0.2	0.03
DS5-1-U2	3.3	0.8	1.6	4.9	8.6	2.1	5.9	3.9	5.7	1.7	0.3	240.0	0.2	0.00
DS5-1-U3	0.3	2.5	0.4	3.0	2.5	12.8	8.6	22.0	7.0	1.7	0.2	380.0	0.4	0.02
DS6-1-O3	7.2	0.7	0.5	5.0	4.4	6.6	5.0	21.1	10.0	0.4	0.4	148.0	0.2	0.05
DS6-1-O2	6.4	0.7	0.5	186.0	22.3	5.8	10.8	22.3	22.0	5.4	0.5	129.0	1.3	0.03
DS6-1-O1	4.0	0.6	2.0	127.0	20.0	5.7	8.6	9.4	22.6	8.3	1.5	113.0	3.9	0.08
DS6-1-T	46.5	0.2	1.3	10.7	5.9	4.0	2.7	14.8	22.3	41.5	6.0	23.6	1.7	0.09
DS6-1-U1	6.8	0.5	1.6	11.2	11.0	5.1	7.8	27.6	12.2	3.9	1.4	170.0	1.6	0.08
DS6-1-U2	9.1	0.7	1.8	6.9	5.2	1.1	3.6	2.5	6.0	1.7	0.7	158.0	0.1	0.03
DS6-1-U3	8.3	0.8	1.6	6.0	5.4	1.2	4.4	3.4	7.2	1.3	0.8	177.0	0.1	0.04
DS6-2s-O3	14.7	1.3	3.1	5.4	5.7	7.3	6.5	4.0	6.5	3.2	0.7	236.0	0.1	0.04
DS6-2s-O2	12.2	1.5	4.1	11.0	11.0	7.4	7.5	25.8	11.3	4.8	2.1	268.0	0.4	0.08
DS6-2s-O1	10.0	1.6	4.6	16.7	16.3	6.5	6.6	10.7	17.9	11.3	4.0	384.0	0.8	0.07
DS6-2s-T	47.0	0.2	1.6	10.5	7.5	2.6	4.9	15.4	28.3	53.3	10.1	114.0	1.5	0.12
DS6-2s-U1	9.2	0.9	2.8	15.1	12.7	9.7	10.3	25.1	20.8	4.2	0.5	194.0	0.3	0.12
DS6-2s-U2	17.1	0.8	2.8	7.8	9.9	5.2	7.4	3.7	17.3	3.7	0.6	210.0	0.1	0.07
DS6-2s-U3	24.9	1.2	2.6	5.0	8.9	3.4	7.5	2.4	9.8	2.3	0.5	290.0	0.1	0.03
DS6-2z-O3	5.3	0.9	0.9	3.2	2.8	8.5	7.5	2.3	5.8	4.4	0.3	653.0	2.1	0.03
DS6-2z-O2	7.1	0.9	1.0	1.9	4.0	6.3	6.3	1.8	5.4	4.0	0.3	670.0	1.1	0.03
DS6-2z-O1	4.2	1.0	2.7	16.1	7.3	11.1	7.7	6.3	11.8	10.2	0.9	614.0	2.1	0.08
DS6-2z-T	30.2	0.3	1.0	9.9	5.6	2.9	3.6	20.3	34.3	27.7	3.7	99.8	2.3	0.17
DS6-2z-U1	9.9	0.5	2.1	20.3	8.1	13.4	9.6	13.1	29.6	20.8	1.2	382.0	4.7	0.23
DS6-2z-U2	5.6	1.0	2.1	8.1	5.8	7.6	7.6	39.9	18.8	7.7	0.4	571.0	2.0	0.10
DS6-2z-U3	6.7	0.6	2.0	5.2	5.7	6.1	6.3	3.5	9.8	4.5	0.3	642.0	0.8	0.03
DS7-O3	6.7	1.5	2.6	4.7	6.8	5.4	8.2	24.6	16.4	2.9	1.2	181.0	0.6	0.00
DS7-O2	10.1	1.6	4.0	6.3	7.8	7.4	10.6	24.8	9.9	3.5	1.7	174.0	1.7	0.04
DS7-O1	12.9	1.7	5.2	20.2	10.0	4.6	9.5	27.1	25.0	14.0	4.4	162.0	4.4	0.11
DS7-T	31.5	0.2	1.9	7.4	2.6	1.4	8.3	7.1	17.0	40.4	3.9	31.4	1.7	0.08
DS7-U1	12.9	1.7	5.1	16.5	9.5	4.9	9.2	26.6	12.7	3.2	0.9	407.0	0.8	0.03
DS7-U2	7.2	1.7	4.2	11.4	8.6	3.3	6.9	3.8	6.9	2.2	0.5	180.0	0.5	0.03
DS7-U3	4.8	1.4	2.6	5.2	10.6	2.8	7.0	3.2	6.1	2.0	0.4	210.0	0.3	0.06
World hard coals*	14.0	2.0	3.7	28.0	6.0	17.0	16.0	28.0	6.0	18.0	100.0	2.1	0.20	
Clay shale†	46.0	2.8	15.0	120.0	76.0	19.0	47.0	36.0	52.0	16.0	130.0	240.0	1.6	1.00
Yan'an Formation coals‡	2.4	8.3	4.6	34.4	31.9	8.2	11.3	6.6	9.5	3.6	0.9	159.0	1.1	0.05

Sample	Sb	Cs	Ba	W	Tl	Pb	Bi	Th	U	Nb	Ta	Zr	Hf
DS3-1-O3	1.21	1.05	42.4	1.23	0.07	4.33	0.30	3.32	5.15	6.47	0.33	50.4	1.45
DS3-1-O2	0.92	0.89	43.5	1.13	0.08	7.99	0.18	5.67	3.97	7.31	0.57	122.0	3.23
DS3-1-O1	0.59	0.63	31.4	0.96	0.09	6.82	0.23	28.80	5.23	20.80	0.90	266.0	3.96
DS3-1-T	1.25	0.68	124.0	0.30	0.05	79.80	1.14	26.90	1.81	9.48	3.19	121.0	10.30
DS3-1-U1	0.43	0.31	22.4	0.77	0.05	3.91	0.13	9.70	5.92	17.60	0.35	125.0	1.98
DS3-1-U2	0.51	0.47	40.8	1.98	0.26	8.45	0.09	2.70	2.78	3.17	0.20	40.5	1.22
DS3-1-U3	0.21	0.02	12.2	1.24	0.01	3.26	0.05	1.06	0.89	0.41	0.04	3.2	0.14
DS5-1-O1	0.86	0.09	8.6	0.15	0.01	3.58	0.18	7.89	3.47	7.28	0.64	57.3	2.38
DS5-1-T	0.59	0.43	16.0	0.55	0.23	30.70	1.30	37.60	1.41	3.06	2.06	79.3	5.14
DS5-1-U1	1.24	0.09	8.1	0.44	0.02	5.96	0.33	10.20	3.06	8.83	0.95	64.8	2.79
DS5-1-U2	0.03	0.06	10.1	0.16	0.00	1.33	0.09	2.33	1.41	1.08	0.09	10.8	0.40
DS5-1-U3	0.24	0.02	8.2	0.59	0.00	0.95	0.04	0.15	0.27	0.14	0.01	1.2	0.05
DS6-1-O3	0.05	0.04	24.7	0.11	0.31	0.79	0.05	1.16	13.20	0.59	0.07	10.2	0.34
DS6-1-O2	0.12	0.04	18.7	0.27	1.02	2.61	0.07	0.71	34.20	0.72	0.09	8.1	0.32
DS6-1-O1	0.71	0.25	14.9	0.61	0.72	3.73	0.22	19.60	51.50	8.14	0.63	84.1	2.31
DS6-1-T	0.16	0.57	30.6	4.33	0.23	21.00	1.29	25.80	9.95	14.90	4.93	105.0	4.89
DS6-1-U1	2.11	0.13	50.0	0.10	0.16	47.40	0.39	15.80	2.96	3.20	0.39	55.8	1.87
DS6-1-U2	0.58	0.05	47.9	0.07	0.00	1.02	0.05	7.95	1.56	1.65	0.07	27.5	1.17
DS6-1-U3	0.03	0.08	98.9	0.09	0.01	1.02	0.04	3.21	1.68	1.78	0.10	30.1	1.19
DS6-2s-O3	0.28	0.05	28.3	0.09	0.01	3.90	0.13	3.83	2.22	2.94	0.14	39.7	1.26
DS6-2s-O2	0.37	0.25	229.0	0.38	0.03	9.18	0.24	15.00	2.44	4.79	0.41	84.0	2.78
DS6-2s-O1	0.35	0.44	3998.0	2.50	0.05	20.70	0.79	60.30	3.35	8.56	1.54	129.0	4.66
DS6-2s-T	0.21	0.83	1701.0	9.03	0.05	11.30	1.11	19.40	4.19	22.60	4.55	104.0	4.80
DS6-2s-U1	0.64	0.04	26.3	0.20	0.01	45.50	0.34	31.80	3.50	3.23	0.61	124.0	4.64
DS6-2s-U2	0.30	0.04	26.2	0.22	0.01	9.85	0.14	14.40	3.61	3.06	0.34	71.0	2.45
DS6-2s-U3	0.14	0.04	33.5	0.11	0.01	5.86	0.09	3.09	4.80	1.47	0.18	28.6	1.09
DS6-2z-O3	0.22	0.02	51.6	0.14	0.11	3.80	0.07	0.72	1.97	0.50	0.06	6.8	0.33

(continued on next page)

Table 5 (continued)

Sample	Sb	Cs	Ba	W	Tl	Pb	Bi	Th	U	Nb	Ta	Zr	Hf
DS6-2z-O2	0.24	0.05	73.6	0.17	0.04	4.20	0.07	0.68	2.01	0.41	0.06	4.6	0.23
DS6-2z-O1	0.33	0.14	31.4	1.19	0.03	13.60	0.27	37.90	5.54	7.73	0.74	105.0	4.01
DS6-2z-T	0.13	0.69	179.0	7.53	0.05	15.70	1.75	28.90	5.62	22.00	5.41	131.0	5.06
DS6-2z-U1	0.51	0.20	12.8	0.35	0.24	23.80	1.31	54.40	5.14	7.22	2.64	242.0	8.74
DS6-2z-U2	0.22	0.05	19.6	0.21	0.01	6.55	0.11	13.30	4.27	5.42	0.13	48.0	1.87
DS6-2z-U3	0.09	0.05	7.1	0.14	0.00	4.85	0.06	3.75	2.67	2.34	0.11	29.5	1.15
DS7-O3	0.17	0.15	15.1	0.20	0.02	3.80	0.26	2.76	4.12	3.29	0.16	23.5	0.88
DS7-O2	0.36	0.21	22.0	0.15	0.15	7.65	0.20	5.43	5.50	4.38	0.18	47.1	1.36
DS7-O1	1.61	0.77	90.9	2.46	0.07	10.00	0.68	29.80	5.34	11.20	0.99	140.0	3.62
DS7-T	0.10	0.73	15.3	4.14	0.04	35.60	1.20	22.10	6.75	20.80	3.36	71.6	5.02
DS7-U1	0.26	0.18	24.1	0.28	0.08	14.70	0.23	17.00	4.16	3.43	0.19	73.9	1.76
DS7-U2	0.06	0.08	9.1	0.13	0.03	3.77	0.10	4.69	3.42	2.45	0.13	45.5	1.35
DS7-U3	0.09	0.09	11.8	0.16	0.01	7.53	0.10	3.37	2.80	1.40	0.11	15.9	0.55
World hard coals*	1.00	1.10	150.0	0.99	0.58	9.00	1.10	3.20	1.90	4.00	0.30	36.0	1.20
Clay shale†	1.00	10.00	460.0	2.60	1.30	14.00	0.38	10.00	4.50	11.00	1.40	190.0	5.00
Yan'an Formation coals‡	0.50	0.11	200.5	0.30	0.10	4.85	0.15	2.95	1.15	1.42	0.06	10.1	0.30

Note: * Ketris and Yudovich (2009); † Grigor'ev (2003); ‡ Wang et al. (2018).

Table 6

REY (rare earth element and Y) concentrations on ash basis (ppm) in tonsteins and enclosing coals.

Sample	La	Ce	Pr	Nd	Sm	Eu	Gd	Tb	Dy	Y	Ho	Er	Tm	Yb	Lu	REY
DS3-1-O3	10.7	22.3	2.94	13.30	3.87	0.93	3.23	0.88	5.87	53.10	1.45	3.91	0.69	4.08	0.76	128.01
DS3-1-O2	10.1	20.1	2.69	12.20	3.08	0.76	2.87	0.69	4.88	42.40	1.17	3.62	0.59	3.50	0.62	109.27
DS3-1-O1	13.3	28.3	3.40	15.40	3.65	0.82	3.08	0.79	5.25	43.20	1.19	3.53	0.56	3.35	0.68	126.50
DS3-1-T	8.9	18.9	2.17	7.87	1.46	0.24	1.09	0.16	0.90	3.62	0.15	0.43	0.06	0.39	0.07	46.35
DS3-1-U1	7.1	14.9	1.91	8.79	2.34	0.55	1.91	0.46	3.23	31.30	0.80	2.13	0.36	2.21	0.40	78.37
DS3-1-U2	7.5	14.6	1.97	8.74	2.23	0.53	1.97	0.46	3.30	31.30	0.77	2.44	0.38	2.37	0.41	79.01
DS3-1-U3	7.3	14.8	1.90	8.29	2.30	0.57	2.08	0.44	3.14	32.20	0.70	2.08	0.29	1.76	0.29	78.17
DS51-O1	4.4	9.1	1.28	6.39	1.91	0.48	1.46	0.44	3.36	21.80	0.74	1.98	0.31	1.88	0.31	55.83
DS5-1-T	10.4	26.8	3.12	12.40	2.66	0.46	1.93	0.40	2.44	12.00	0.41	1.31	0.17	1.17	0.21	75.87
DS5-1-U1	4.0	8.4	1.13	5.46	1.54	0.40	1.53	0.37	2.66	18.90	0.64	1.65	0.29	1.71	0.30	48.96
DS5-1-U2	10.1	20.2	2.27	7.75	1.44	0.29	1.31	0.23	1.41	9.07	0.31	0.94	0.15	1.06	0.17	56.70
DS51-U3	1.9	4.3	0.62	3.10	0.83	0.19	0.78	0.20	1.44	11.20	0.32	0.89	0.14	0.94	0.14	27.00
DS61-O3	0.9	2.2	0.38	1.66	0.42	0.08	0.30	0.08	0.38	2.80	0.08	0.27	0.03	0.29	0.04	9.93
DS61-O2	1.9	4.2	0.73	3.19	0.88	0.12	0.62	0.13	0.78	5.23	0.15	0.49	0.09	0.52	0.08	19.13
DS61-O1	9.6	21.8	2.97	11.00	1.97	0.32	1.74	0.33	1.78	8.97	0.34	1.13	0.16	1.13	0.19	63.39
DS61-T	23.7	52.0	5.30	18.30	2.60	0.28	2.20	0.29	1.35	3.34	0.15	0.60	0.06	0.52	0.07	110.75
DS6-1-U1	7.0	15.5	1.88	6.14	1.16	0.13	0.81	0.15	0.77	2.76	0.12	0.39	0.07	0.30	0.06	37.21
DS61-U2	4.0	9.1	1.26	4.81	1.07	0.15	0.71	0.13	0.84	3.40	0.14	0.38	0.07	0.43	0.08	26.54
DS6-1-U3	3.6	8.6	1.14	4.46	1.04	0.18	0.76	0.14	0.86	3.90	0.15	0.44	0.08	0.53	0.08	25.91
DS6-2s-O3	0.8	3.5	0.66	2.94	0.86	0.14	0.58	0.16	1.24	6.34	0.24	0.78	0.17	1.03	0.14	19.59
DS6-2s-O2	1.3	4.8	0.88	3.52	1.05	0.19	0.70	0.22	1.34	7.76	0.29	0.96	0.17	1.11	0.19	24.48
DS6-2s-O1	5.4	16.0	2.09	7.51	1.69	0.61	1.24	0.27	1.50	7.71	0.29	1.08	0.19	1.10	0.20	46.92
DS6-2s-T	3.5	9.8	1.27	4.70	0.82	0.07	0.68	0.11	0.70	2.29	0.11	0.34	0.06	0.40	0.05	24.90
DS6-2s-U1	1.8	6.2	0.97	4.29	0.96	0.14	0.66	0.16	0.89	5.23	0.20	0.63	0.12	0.74	0.12	23.13
DS62s-U2	2.4	8.3	1.31	5.89	1.35	0.24	1.02	0.18	1.28	7.32	0.27	0.83	0.14	0.85	0.14	31.44
DS6-2s-U3	3.7	13.9	2.28	11.00	2.69	0.46	1.72	0.37	2.31	12.40	0.40	1.24	0.18	1.23	0.17	54.07
DS6-2z-O3	1.3	3.7	0.62	2.68	0.74	0.12	0.61	0.13	0.90	4.64	0.17	0.54	0.09	0.50	0.11	16.86
DS6-2z-O2	1.3	3.7	0.55	2.65	0.68	0.13	0.48	0.12	0.81	4.34	0.14	0.43	0.07	0.47	0.09	15.94
DS6-2z-O1	3.2	8.5	1.19	4.68	1.13	0.18	0.84	0.18	1.15	5.70	0.23	0.66	0.12	0.85	0.13	28.79
DS6-2z-T	15.9	35.4	3.73	12.70	1.74	0.23	1.64	0.24	1.18	3.07	0.14	0.48	0.06	0.43	0.07	77.00
DS6-2z-U1	13.2	32.0	3.57	12.00	2.11	0.26	1.81	0.24	1.38	5.02	0.22	0.67	0.10	0.76	0.10	73.45
DS6-2z-U2	2.2	6.5	0.96	4.03	0.92	0.12	0.64	0.14	0.91	4.56	0.17	0.54	0.11	0.68	0.12	22.51
DS6-2z-U3	2.1	5.7	0.90	3.68	0.92	0.14	0.69	0.14	0.98	5.03	0.16	0.57	0.11	0.68	0.10	21.90
DS7-O3	10.1	20.0	2.20	8.41	1.69	0.30	1.48	0.30	1.84	12.70	0.37	1.15	0.22	1.74	0.26	62.75
DS7-O2	9.2	19.1	2.08	7.73	1.44	0.27	1.37	0.25	1.61	9.90	0.31	0.98	0.21	1.33	0.21	55.97
DS7-O1	25.4	50.2	4.72	15.40	2.43	0.40	2.39	0.42	2.26	12.50	0.45	1.50	0.26	1.66	0.31	120.30
DS7-T	21.2	43.4	3.82	11.10	1.46	0.18	1.58	0.22	1.03	3.12	0.13	0.57	0.06	0.52	0.08	88.47
DS7-U1	10.2	21.4	2.42	8.70	1.77	0.29	1.60	0.26	1.62	10.30	0.34	1.12	0.21	1.38	0.24	61.86
DS7-U2	8.8	18.0	2.08	7.39	1.54	0.24	1.31	0.24	1.50	9.00	0.28	1.02	0.19	1.28	0.23	53.07
DS7-U3	8.7	17.3	1.99	7.23	1.46	0.26	1.25	0.23	1.41	8.64	0.28	0.99	0.16	1.19	0.19	51.31
World hard coals*	11.0	23.0	3.40	12.00	2.20	0.43	2.70	0.31	2.10	8.20	0.57	1.00	0.30	1.00	0.20	68.41
Clay shale†	48.0	75.0	10.00	36.00	8.00	1.20	5.80	0.83	4.40	31.00	0.70	1.90	0.60	2.50	0.39	226.32
Yan'an Formation coals‡	3.4	8.5	1.11	4.91	1.43	0.42	1.63	0.38	2.39	17.60	0.58	1.56	0.25	1.41	0.22	45.71

Note: * Ketris and Yudovich (2009); † Grigor'ev (2003); ‡ Wang et al. (2018).

felsic composition. Therefore, high smectite (18%) content detected in the sample DS3-1-T (Table 2) may be caused by the depositional environment or degree of alteration (Dai et al., 2017).

5.3. Leaching of the tonsteins within coal seams

In some cases, tonsteins within coal seams have been leached by groundwaters or hydrothermal solutions, resulting in the enrichment of some trace elements in the underlying and overlying coal benches

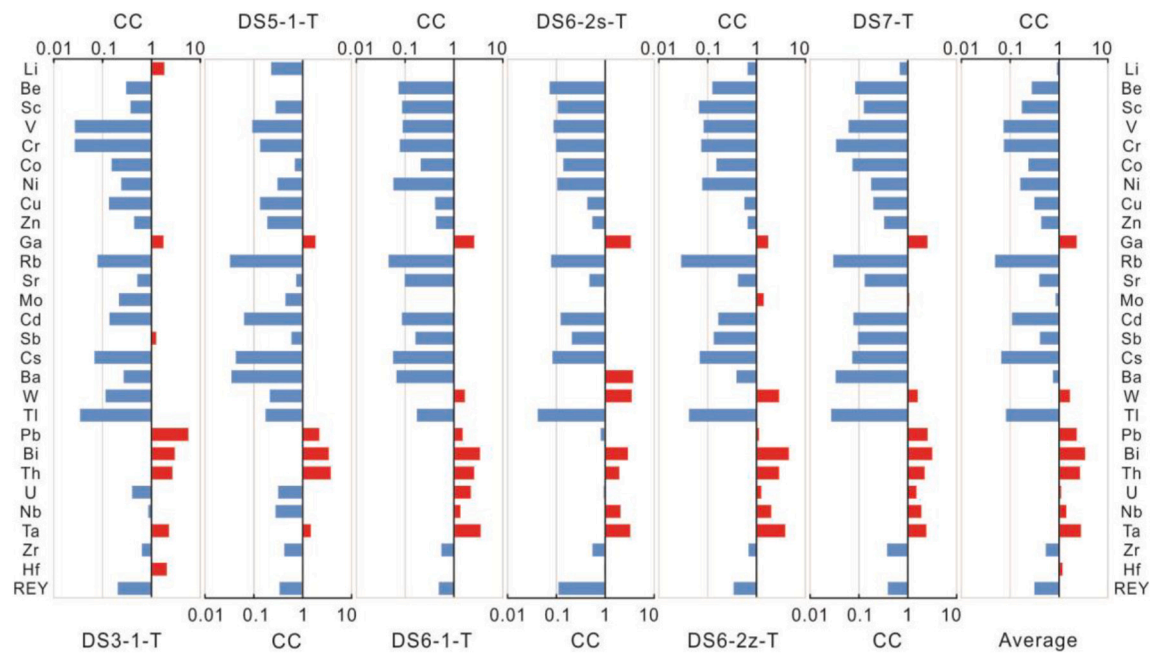


Fig. 9. Concentration coefficients (CC) of trace elements in tonsteins, normalized by the mean composition of clay shale (Grigor'ev, 2003).

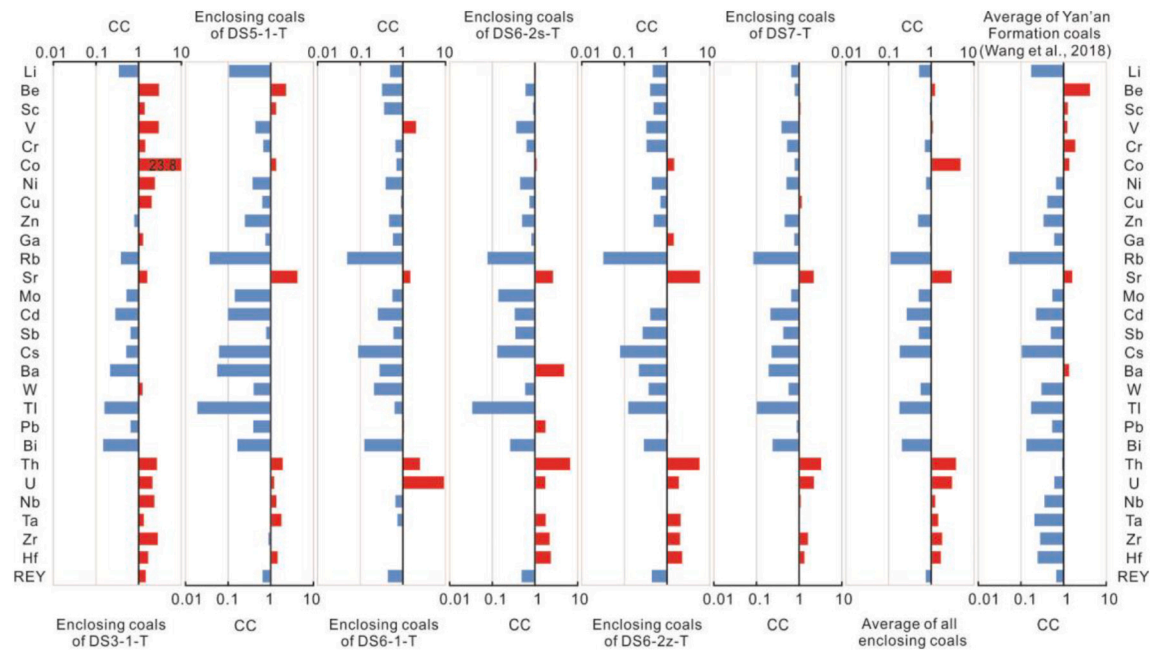


Fig. 10. Concentration coefficients (CC) of enclosing coals both above and below the tonsteins, normalized by the average concentrations of trace elements for world hard coal (Ketris and Yudovich, 2009).

(Arbuзов et al., 2016, 2018; Crowley et al., 1989; Dai et al., 2006, 2013, 2014a; Eskenazy, 2006; Ketris and Yudovich, 2009; Hower et al., 1999; Kalkreuth et al., 2006; Spears and Arbuзов, 2019; Spears et al., 1988; Zhao et al., 2015). For example, Arbuзов et al. (2016) found that highly-elevated concentrations of lanthanides, thorium, uranium, and tantalum are characteristic of the coal immediately above and below the tonsteins that may be related to the leaching of the felsic tonsteins. Wang et al. (2018) indicated that only elements of Be, Sc, V, Cr, Co, Sr, and Ba are enriched in the Yan'an Formation "normal" coals that are without volcanic ash (Fig. 10), compared with the average values for world hard coals (Ketris and Yudovich, 2009). However, the enclosing coals of the tonsteins in the Yan'an Formation have evident anomalously elevated

Th, U, Nb, Ta, Zr, and Hf (Fig. 10), which may be attributed to the leaching of the tonsteins by groundwaters or hydrothermal solutions (Dai et al., 2017). Compared with the mean composition of clay shale (Grigor'ev, 2003), the studied tonsteins are characterized by the high concentrations of the elements mentioned above (Fig. 9). Moreover, compared with the average trace element concentrations of the Mesozoic rhyolites in the North China craton (Gou et al., 2013), the studied tonsteins are depleted in elements Th, U, Nb, Zr, and Hf (Fig. 13), supporting these elements were leached into the enclosing coal. However, only DS5-1-T obviously shows depletion in Ta (Fig. 13), which may be caused by inaccurate equivalent rhyolites of the possible sources. In addition, the elevated concentrations of Co, Ni, Cu, and Sr in the studied

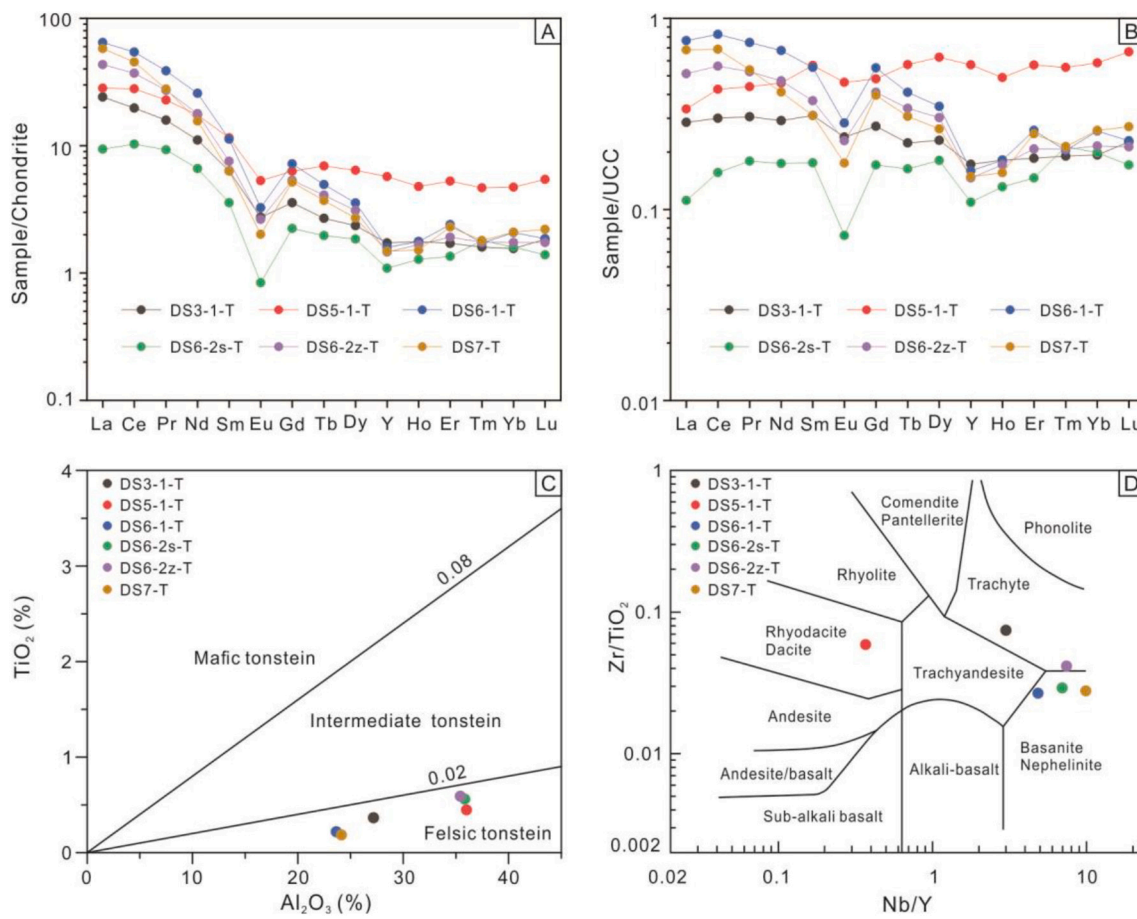


Fig. 11. (A) Chondrite-normalized REY distribution patterns for the tonsteins. Chondrite values are from Taylor and McLennan (1985). (B) UCC-normalized REY distribution patterns for the tonsteins. Upper Continental Crust values are from Taylor and McLennan (1985). (C) TiO₂ versus Al₂O₃ discrimination diagram for the tonsteins (Dai et al., 2011). (D) Zr/TiO₂ versus Nb/Y classification diagram for the tonsteins (Winchester and Floyd, 1977).

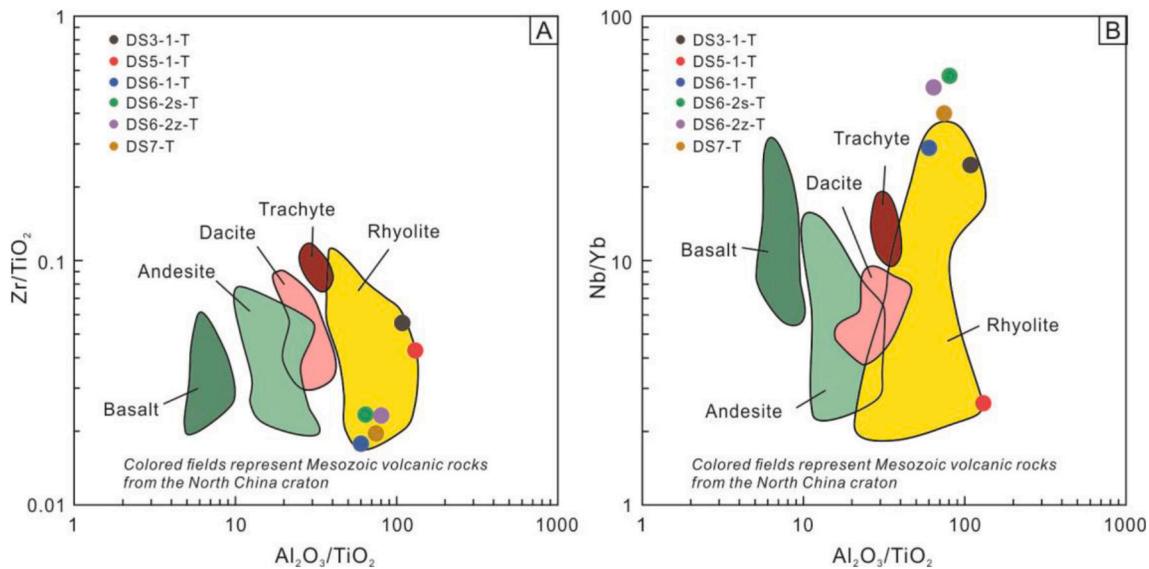


Fig. 12. The Zr/TiO₂ versus Al₂O₃/TiO₂ and Nb/Yb versus Al₂O₃/TiO₂ diagrams for the tonsteins. Colored fields represent Mesozoic volcanic rocks from the North China craton (Chang et al., 2020; Gou et al., 2013; Han et al., 2020; He et al., 2017; Wang et al., 2015; Wu et al., 2021; Yang et al., 2018; Zhang et al., 2014).

tonsteins may be sourced by the acidic solutions (Fig. 13), which can also be responsible for leaching of Be, Rb, Cs, Th, U, Nb, Zr, Hf, and REY (Dai et al., 2017; Nechaev et al., 2021). The evidence of above elements

released from the parent ash during the alteration process indicates that these elements are not only hosted in resistate minerals, such as zircon and phosphate minerals, but may be contained in volcanic glass or less

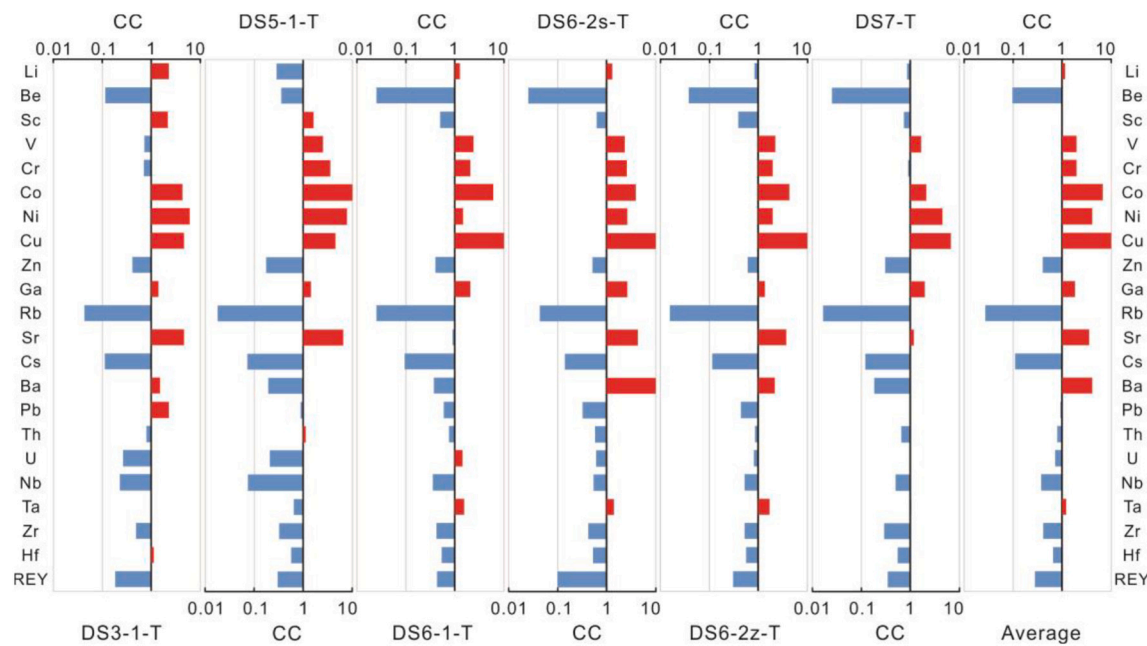


Fig. 13. Concentration coefficients (CC) of trace elements in tonsteins, normalized by average trace element concentrations of the Mesozoic rhyolites in the North China craton (Gou et al., 2013).

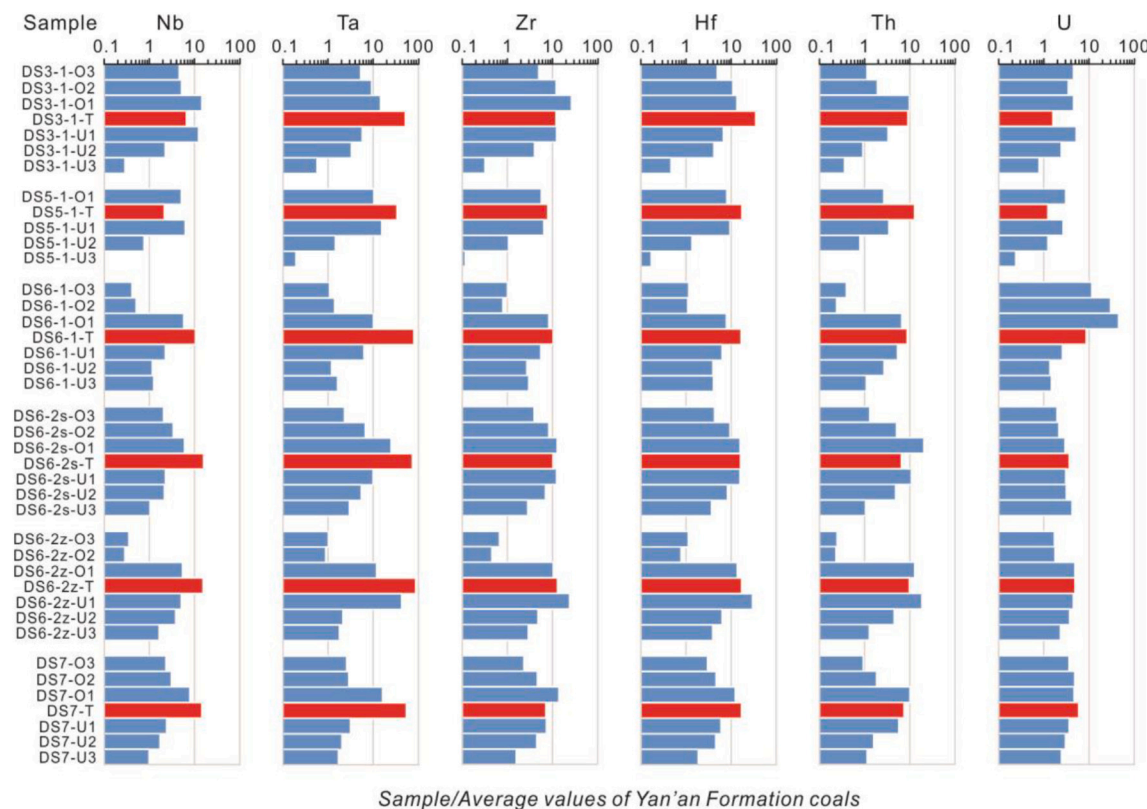


Fig. 14. The vertical variation of concentration coefficients (CC) for trace elements Nb, Ta, Zr, Hf, Th, and U in the tonsteins and enclosing coals, normalized by average trace element concentrations of Yan'an Formation coals (Wang et al., 2018).

stable minerals (Zhou et al., 2000; Zhao et al., 2017; Dai et al., 2017; Spears and Arbuzov, 2019). It is also noted that mobility of these elements would impose some constraints on the use of corresponding discrimination diagrams for the interpretation of original ash composition and tectonic setting (Spears and Arbuzov, 2019).

Moreover, to investigate the mobile distance of the elements from

the tonsteins into its overlying and underlying coals, the element concentrations in the tonsteins and enclosing coals have been normalized to the average values of the Yan'an Formation coals (Wang et al., 2018). As shown in Fig. 14, apart from the DS3-1-T and DS5-1-T, almost all other tonsteins (DS6-1-T, DS6-2s-T, DS6-2z-T, and DS7-T) have an enrichment width of up to 30 cm for elements Th, U, Nb, Ta, Zr, and Hf into its

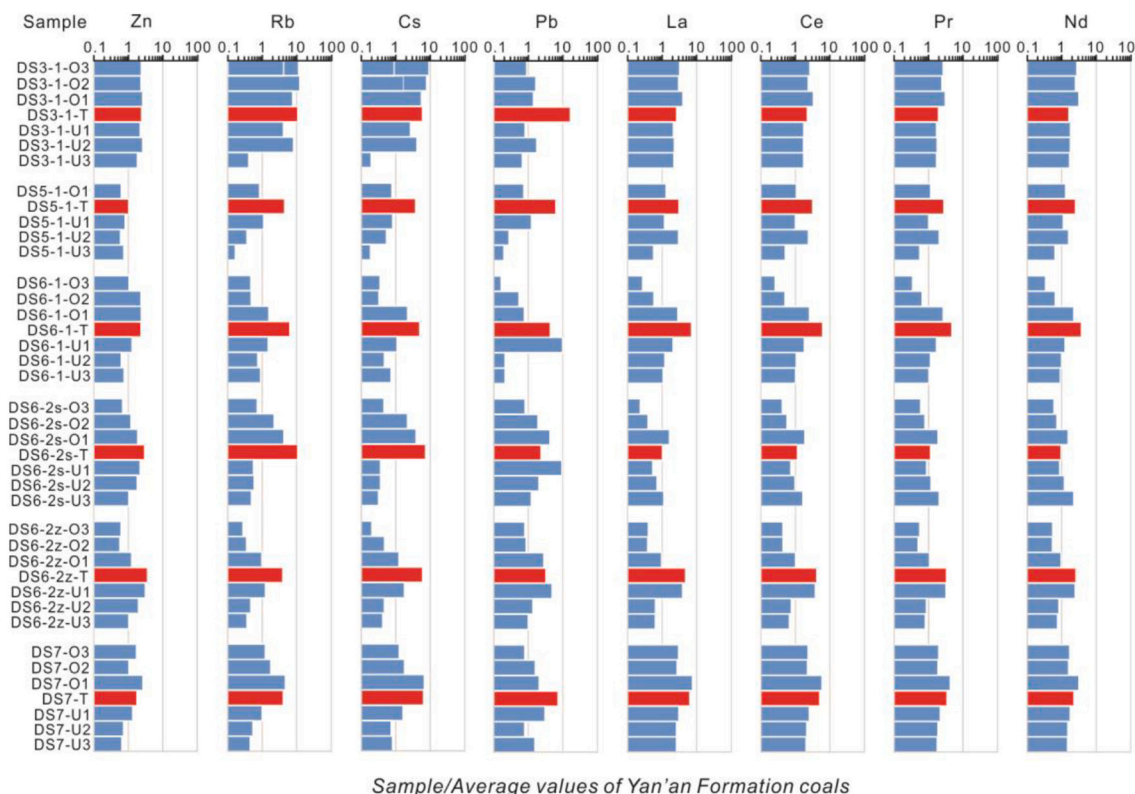


Fig. 15. The vertical variation of concentration coefficients (CC) for trace elements of Zn, Rb, Cs, Pb, La, Ce, Pr, and Nd in the tonsteins and enclosing coals, normalized by average trace element concentrations of Yan'an Formation coals (Wang et al., 2018).

adjacent coals, and showing the concentrations decreasing with the distance from the tonsteins (Fig. 13). The DS3-1-T and DS5-1-T only have a narrower enrichment zone (~ 20 cm) in the enclosing coals, possibly due to their thinner thicknesses (1.3 cm for the DS3-1-T and 0.2 cm for the DS5-1-T). It is worth noting that the distance of leaching tonsteins into the underlying coals is longer than the overlying coals, such as the overlying coals in the DS6-1-T and DS6-2z-T only with a 10 cm enrichment zone (Fig. 13).

Although a number of elements (e.g., Zn, Rb, Cs, and Pb) are also depleted in the tonsteins (Fig. 13), the coal seams both above and below the tonsteins do not have enrichment in these elements (Fig. 10). Except for some directly underlying and overlying coals (e.g., DS6-2s-O1, DS6-2s-U1, DS6-2z-O1, DS6-2z-U1, and DS7-O1) with less elevated concentrations of the above-mentioned elements (Fig. 15). This may be caused by the mobility of the elements and the character of interaction between the tonsteins and adjacent coals (Arbuzov et al., 2016). Moreover, Hower et al. (1999) and Arbuzov et al. (2016) identified that elevated concentrations of lanthanides in the enclosing coals due to the leaching of the felsic volcanic ashes that also can be served as the roof strata (Ketris and Yudovich, 2009). In this study, possible leaching of lanthanides, such as La, Ce, Pr, and Nd, from the tonsteins and retention in the adjacent coals, especially the coals in immediate contact with the tonsteins, have also been recognized (Fig. 15).

6. Conclusions

Based on petrographic, mineralogical, geochemical, and zircon U—Pb geochronology analyses of six tonsteins and their enclosing coals from the Middle Jurassic Yan'an Formation of the Ordos Basin, north-eastern China, we mainly suggested the following conclusions:

(1) The line of typical evidence including thin beds, distinct lateral continuity with paler color and sharp contacts, vermicular kaolinite, and angular quartz crystals, and euhedral zircons with similar U—Pb ages

indicates a significant pyroclastic origin of the tonsteins within coal seams in the Yan'an Formation. However, rounded quartz, muscovite, and detrital zircon grains reflect minor contribution of terrigenous debris for the tonsteins.

(2) The felsic (rhyolite) composition for the initial volcanogenic material of the tonsteins has been confirmed by both the mineralogical and geochemical characteristics. The presence of sanidine may imply a felsic to intermediate source magma. Particularly, the tonsteins have low TiO_2/Al_2O_3 ratios (<0.02), plotting Al_2O_3/TiO_2 against Nb/Yb , and Zr/TiO_2 situated in or near the rhyolite field, and relatively lower REY concentrations with pronounced negative Eu anomalies, but a greater fractionation between LREY and HREY.

(3) The elevated concentrations of the enclosing coals in elements Th, U, Nb, Ta, Zr, and Hf are attributed to leaching from the tonsteins with mobile distance reached up 30 cm. Moreover, elements of Zn, Rb, Cs, Pb and some of lanthanides including La, Ce, Pr, and Nd can also have mobility with loss from the tonsteins and retention in a relatively narrow zone of the overlying and underlying coals. The width of the enrichment in the adjacent coals may be associated with the properties of the tonsteins, such as the thickness and original magma source, the features of the elements, e.g., mobility and initial concentration, and the character of interaction between the tonsteins and enclosing coals.

Declaration of Competing Interest

We declare that we have no conflict of interest.

Acknowledgments

We would like to thank Editor-in-Chief Prof. Shifeng Dai, D.A. Spears, Victor Nечаev and the other anonymous reviewer for their constructive comments. This study was financially supported by the National Natural Science Foundation of China (41772096, 42102127,

42172117), Shandong Provincial Natural Science Foundation (ZR2021QD087), Chinese Postdoctoral Science Foundation (2021M702019), SDUST Research Fund (2018TDJH101), and National Key Research and Development Project (2019YFC0605403).

References

- Admakin, L., Portnov, A., 1987. Tonsteins of Irkutsk basin [in Russian: Tonshtejny Irkutskogo bassejna]. Litol. Pol. Iskop. 3, 88–98.
- Altaner, S.P., Grim, R.E., 1990. Mineralogy, chemistry, and diagenesis of tuffs in the Sucker Creek Formation (Miocene), eastern Oregon. Clay Clay Miner. 38, 561–572.
- Anggara, F., Amijaya, D.H., Harijoko, A., Tambaria, T.N., Sahri, A.A., Asa, Z.A.N., 2018. Rare earth element and yttrium content of coal in the Banko coalfield, South Sumatra Basin, Indonesia: Contributions from tonstein layers. Int. J. Coal Geol. 196, 159–172.
- Ao, W., Huang, W., Weng, C., Xiao, X., Liu, D., Tang, X., Chen, P., Zhao, Z., Wan, H., Finkelman, R.B., 2012. Coal petrology and genesis of Jurassic coal in the Ordos Basin, China. Geosci. Front. 3, 85–95.
- Arbuzov, S.I., Mezhibor, A.M., Spears, D., Ilenok, S.S., Shaldybin, M.V., Belyayev, E., 2016. Nature of tonsteins in the Azeisk deposit of the Irkutsk Coal Basin (Siberia, Russia). Int. J. Coal Geol. 153, 99–111.
- Arbuzov, S., Maslov, S., Finkelman, R., Mezhibor, A., Ilenok, S., Blokhin, M., Peregudina, E., 2018. Modes of occurrence of rare earth elements in peat from Western Siberia. J. Geochem. Explor. 184, 40–48.
- Bau, M., Schmidt, K., Koschinsky, A., Hein, J., Kuhn, T., Usui, A., 2014. Discriminating between different genetic types of marine ferro-manganese crusts and nodules based on rare earth elements and yttrium. Chem. Geol. 381, 1–9.
- Bohor, B.F., Triplehorn, D.M., 1993. Tonsteins: altered volcanic-ash layers in coal-bearing sequences. Geol. Soc. Am. Spec. Pap. 285, 44.
- Boucou, A.J., Xu, C., Scotese, C.R., Morley, R.J., 2013. Phanerozoic Paleoclimate: An Atlas of Lithologic Indicators of Climate: Tulsa Oklahoma, SEPM (Society for Sedimentary Geology) Concepts in Sedimentology and Paleontology Series, 11.
- Bouroz, A., 1967. Correlations des tonsteins d'origine volcanique entre les bassins houillers de Sarre-Lorraine et du Nord-Pas-de-Calais. Compte Rendu Hebdomadaire des Séances de l'Academie des Sciences Serie D Science Naturelle, Paris 264, 2729–2732.
- Bouroz, A., Spears, D.A., Arbe, F., 1983. Essai de synthèse des données acquises sur la genèse et l'évolution des marqueurs pétrographiques dans les bassins houillers. In: Mémoire XVI. Société Géologique du Nord, 114 pp.
- Burger, K., Damberger, H.H., 1985. Tonsteins in the coalfields of western Europe and North America. In: Cross, A.T. (Ed.), Compte Rendu of 9th International Conference on Carboniferous Stratigraphy and Geology, Washington, D.C. and Champaign-Urbana, May 1979. Southern Illinois Univ. Press, Carbondale, pp. 433–448. Economic Geology—Coal, Oil and Gas 4.
- Chang, Z., Dong, G., Mo, X., Dong, P., Li, H., 2020. Early cretaceous bimodal volcanic rocks in the Yinchuan belt, North China Craton: age, petrogenesis, and geological significance. Int. J. Earth Sci. 109, 2189–2207.
- Chekin, S., 1973. Lower Mesozoic Weathering Crust of Irkutskiy Amphitheatre [in Russian: Nizhnemezozojskaja Kora Vyvetrivanija Irkutskogo Amfiteatral]. Nauka, Moscow, p. 156.
- China National Administration of Coal Geology, 1996. Coal Accumulating and Coal Resource Evaluation of Ordos Basin. China Coal Industry Publishing House, Beijing (in Chinese with English abstract).
- Crowley, S.S., Stanton, R.W., Ryer, T.A., 1989. The effects of volcanic ash on the maceral and chemical composition of the C coal bed, Emery Coal Field, Utah. Org. Geochem. 14, 315–331.
- Dai, S., Ren, D., Hou, X., Shao, L., 2003. Geochemical and mineralogical anomalies of the late Permian coal in the Zhijin coalfield of southwest China and their volcanic origin. Int. J. Coal Geol. 55, 117–138.
- Dai, S., Ren, D., Chou, C.L., Li, S., Jiang, Y., 2006. Mineralogy and geochemistry of the no. 6 coal (Pennsylvanian) in the Junger Coalfield, Ordos Basin, China. Int. J. Coal Geol. 66 (4), 253–270.
- Dai, S., Wang, X., Chen, W., Li, D., Chou, C.-L., Zhou, Y., Zhu, C., Li, H., Zhu, X., Xing, Y., 2010. A high-pyrite semiantarctite of Late Permian age in the Songzao Coalfield, southwestern China: Mineralogical and geochemical relations with underlying mafic tuffs. Int. J. Coal Geol. 83, 430–445.
- Dai, S., Wang, X., Zhou, Y., Hower, J.C., Li, D., Chen, W., Zhu, X., Zou, J., 2011. Chemical and mineralogical compositions of silicic, mafic, and alkali tonsteins in the late Permian coals from the Songzao Coalfield, Chongqing, Southwest China. Chem. Geol. 282, 29–44.
- Dai, S., Zhang, W., Ward, C.R., Seredin, V.V., Hower, J.C., Li, X., Song, W., Wang, X., Kang, H., Zheng, L., Wang, P., 2013. Mineralogical and geochemical anomalies of late Permian coals from the Fusui Coalfield, Guangxi Province, southern China: influences of terrigenous materials and hydrothermal fluids. Int. J. Coal Geol. 105, 60–84.
- Dai, S., Guo, W., Nechaev, V.P., French, D., Ward, C.R., Spiro, B.F., Finkelman, R.B., 2018. Modes of occurrence and origin of mineral matter in the Palaeogene coal (No. 19-2) from the Hunchun Coalfield, Jilin Province, China. Int. J. Coal Geol. 189, 94–110.
- Dai, S., Li, T., Seredin, V.V., Ward, C.R., Hower, J.C., Zhou, Y., Zhang, M., Song, X., Song, W., Zhao, C., 2014a. Origin of minerals and elements in the Late Permian coals, tonsteins, and host rocks of the Xinde Mine, Xuanwei, eastern Yunnan, China. Int. J. Coal Geol. 121, 53–78.
- Dai, S., Luo, Y., Seredin, V.V., Ward, C.R., Hower, J.C., Zhao, L., Liu, S., Zhao, C., Tian, H., Zou, J., 2014b. Revisiting the late Permian coal from the Huayingshan, Sichuan, southwestern China: Enrichment and occurrence modes of minerals and trace elements. Int. J. Coal Geol. 122, 110–128.
- Dai, S., Seredin, V.V., Ward, C.R., Hower, J.C., Xing, Y., Zhang, W., Song, W., Wang, P., 2015. Enrichment of U-Se-Mo-Re-V in coals preserved within marine carbonate successions: geochemical and mineralogical data from the Late Permian Guiding Coalfield, Guizhou, China. Mineral. Deposita 50 (2), 159–186.
- Dai, S., Graham, I.T., Ward, C.R., 2016. A review of anomalous rare earth elements and yttrium in coal. Int. J. Coal Geol. 159, 82–95.
- Dai, S., Ward, C.R., Graham, I.T., French, D., Hower, J.C., Zhao, L., Wang, X., 2017. Altered volcanic ashes in coal and coal-bearing sequences: a review of their nature and significance. Earth Sci. Rev. 175, 44–74.
- Dai, S., Finkelman, R.B., French, D., Hower, J.C., Graham, I.T., Zhao, F., 2021. Modes of occurrence of elements in coal: a critical evaluation. Earth Sci. Rev. 222, 103815.
- Darby, B.J., Ritts, B.D., 2002. Mesozoic contractional deformation in the middle of the Asian tectonic collage: the intraplate Western Ordos fold-thrust belt, China. Earth Planet. Sci. Lett. 205, 13–24.
- Erkoyun, H., Kadir, S., Huggett, J., 2019. Occurrence and genesis of tonsteins in the Miocene lignite, Tunçbilek Basin, Kütahya, western Turkey. Int. J. Coal Geol. 202, 46–68.
- Eskenazy, G.M., 2006. Geochemistry of beryllium in Bulgarian coals. Int. J. Coal Geol. 66, 305–315.
- Finkelman, R.B., 1994. Modes of occurrence of potentially hazardous elements in coal: levels of confidence. Fuel Process. Technol. 39, 21–34.
- Goodarzi, F., Sanei, H., Stasiuk, L., Bagheri-Sadeghi, H., Reyes, J., 2006. A preliminary study of mineralogy and geochemistry of four coal samples from northern Iran. Int. J. Coal Geol. 65, 35–50.
- Gou, J., Sun, D.Y., Liu, Y.J., Ren, Y.S., Zhao, Z.H., Liu, X.M., 2013. Geochronology, petrogenesis, and tectonic setting of Mesozoic volcanic rocks, southern Manzhouli area, Inner Mongolia. Int. Geol. Rev. 55 (8), 1029–1048.
- Grigor'ev, N., 2003. Average concentrations of chemical elements in rocks of the upper continental crust. Geochim. Int. 41, 711–718.
- Guerra-Sommer, M., Cazzullo-Klepzig, M., Formoso, M.L.L., Menegat, R., Fo, J.G.M., 2008. U-Pb dating of tonstein layers from a coal succession of the southern Paraná Basin (Brazil): a new geochronological approach. Gondwana Res. 14, 474–482.
- Han, Z., Ren, X., Schertl, H.-P., Li, X.-P., Song, Z.-G., Du, Q.-X., Han, C., Zhong, W.-J., Gao, L.-H., 2020. Zircon U-Pb-Hf isotopes and geochemistry of Jurassic igneous rocks from the southern Zhangguangcai Range, NE China: constraints on magmatism, petrogenesis and tectonic implications. Int. Geol. Rev. 62, 1988–2012.
- Hayashi, K.-I., Fujisawa, H., Holland, H.D., Ohmoto, H., 1997. Geochemistry of ~1.9 Ga sedimentary rocks from northeastern Labrador, Canada. Geochim. Cosmochim. Acta 61, 4115–4137.
- He, X., Santosh, M., Ganguly, S., 2017. Mesozoic felsic volcanic rocks from the North China craton: Intraplate magmatism associated with craton destruction. Geol. Soc. Am. Bull. 129, 947–969.
- Hong, H., Algeo, T.J., Fang, Q., Zhao, L., Ji, K., Yin, K., Wang, C., Cheng, S., 2019. Facies dependence of the mineralogy and geochemistry of altered volcanic ash beds: an example from Permian-Triassic transition strata in southwestern China. Earth Sci. Rev. 190, 58–88.
- Hower, J.C., Ruppert, L.F., Eble, C.F., 1999. Lanthanide, yttrium, and zirconium anomalies in the Fire Clay coal bed, Eastern Kentucky. Int. J. Coal Geol. 39, 141–153.
- Hower, J.C., Eble, C.F., Dai, S., Belkin, H.E., 2016. Distribution of rare earth elements in eastern Kentucky coals: indicators of multiple modes of enrichment? Int. J. Coal Geol. 160, 73–81.
- Hower, J.C., Berti, D., Hochella Jr., M.F., Mardon, S.M., 2018. Rare earth minerals in a “no tonstein” section of the Dean (Fire Clay) coal, Knox County, Kentucky. Int. J. Coal Geol. 193, 73–86.
- Johnson, E.A., Liu, S., Zhang, Y., 1989. Depositional environments and tectonic controls on the coal-bearing Lower to Middle Jurassic Yan'an Formation, southern Ordos Basin, China. Geology 17, 1123–1126.
- Kalkreuth, W., Holz, M., Kern, M., Machado, G., Mexias, A., Silva, M., Willett, J., Finkelman, R., Burger, H., 2006. Petrology and chemistry of Permian coals from the Paraná Basin: 1. Santa Terezinha, Leão-Butiá and Candiota Coalfields, Rio Grande do Sul, Brazil. Int. J. Coal Geol. 68, 79–116.
- Karayigit, A.I., Atalay, M., Oskay, R.G., Córdoba, P., Querol, X., Bulut, Y., 2020a. Variations in elemental and mineralogical compositions of Late Oligocene, Early and Middle Miocene coal seams in the Kale-Tavas MOLASSE sub-basin, SW Turkey. Int. J. Coal Geol. 218, 103366.
- Karayigit, A.I., Bircan, C., Oskay, R.G., Türkmen, İ., Querol, X., 2020b. The geology, mineralogy, petrography, and geochemistry of the Miocene Dursunbey coal within fluvio-lacustrine deposits, Balıkesir (Western Turkey). Int. J. Coal Geol. 228, 103548.
- Ketris, M.Á., Yudovich, Y.E., 2009. Estimations of Clarkes for Carbonaceous biolithes: world averages for trace element contents in black shales and coals. Int. J. Coal Geol. 78, 135–148.
- Li, S., Cheng, S., Yang, S., 1992. Sequence Stratigraphy and Depositional System Analysis of the Northeastern Ordos Basin. Geological Publishing House, Beijing (in Chinese with English abstract).
- Liu, J., Nechaev, V.P., Dai, S., Song, H., Nechaeva, E.V., Jiang, Y., Graham, I.T., French, D., Yang, P., Hower, J.C., 2020. Evidence for multiple sources for inorganic components in the Tucheng coal deposit, western Guizhou, China and the lack of critical-elements. Int. J. Coal Geol. 223, 103468.
- Lyons, P.C., Krogh, T., Kwok, Y., Davis, D.W., Outerbridge, W.F., Evans Jr., H.T., 2006. Radiometric ages of the Fire Clay tonstein [Pennsylvanian (Upper Carboniferous),

- Westphalian, Duckmantian]: A comparison of U-Pb zircon single-crystal ages and 40Ar/39Ar sanidine single-crystal plateau ages. *Int. J. Coal Geol.* 67, 259–266.
- Mardon, S.M., Hower, J.C., 2004. Impact of coal properties on coal combustion by-product quality: examples from a Kentucky power plant. *Int. J. Coal Geol.* 59, 153–169.
- Mikheeva, E.A., Demonterova, E.I., Khubanov, V.B., Ivanov, A.V., Arzhannikova, A.V., Arzhannikov, S.G., Blinov, A.V., 2020. Age of the coal accumulation in the Irkutsk basin based on accessory zircon dating in the Azeisk deposit tonstein (LA-ICP-MS). *Vestnik of Saint Petersburg University. Earth Sci.* 65, 420–433.
- Möeller, P., 2000. Rare earth elements and yttrium as geochemical indicators of the source of mineral and thermal waters. In: Stober, I., Bucher, K. (Eds.), *Hydrogeology of Crystalline Rocks*. Springer, pp. 227–246.
- Nechaev, V.P., Dai, S., Chekryzhev, I.Y., Tarasenko, I.A., Zin'kov, A.V., Moore, T.A., 2021. Origin of the tuff parting and associated enrichments of Zr, REY, redox-sensitive and other elements in the early Miocene coal of the Siniy Utys Basin, southwestern Primorye, Russia. *Int. J. Coal Geol.* 103913.
- Oskay, R.G., Bechtel, A., Karayigit, A.I., 2019. Mineralogy, petrography and organic geochemistry of Miocene coal seams in the Kinik coalfield (Soma Basin-Western Turkey): insights into depositional environment and palaeo-vegetation. *Int. J. Coal Geol.* 210, 103205.
- Reinink-Smith, L.M., 1990. Mineral assemblages of volcanic and detrital partings in Tertiary coal beds, Kenai Peninsula, Alaska. *Clay Clay Miner.* 38, 97–108.
- Rice, C., Belkin, H., Kunk, M., Henry, T., 1990. Distribution, stratigraphy, mineralogy, and 40Ar/39Ar age spectra of the Middle Pennsylvanian Fire Clay tonstein of the central Appalachian Basin. *Geol. Soc. Am. Abstr. Programs* A320–A321.
- Ruppert, L.F., Moore, T.A., 1993. Differentiation of volcanic ash-fall and water-borne detrital layers in the Eocene Senakin coal bed, Tanjung Formation, Indonesia. *Org. Geochem.* 20, 233–247.
- Seredin, V.V., Dai, S., 2012. Coal deposits as potential alternative sources for lanthanides and yttrium. *Int. J. Coal Geol.* 94, 67–93.
- Sha, J., Chen, J., Zhang, B., Chen, P., Zhang, S., Zeng, J., Liu, W., Wang, X., Zhang, P., Yao, D., 2020. Geochemistry of source rock-controlled Late Triassic coal: an example from the Dabaoding Coal Mine in Panzhihua, Sichuan Province, southwestern China. *Int. J. Coal Geol.* 221, 103431.
- Shen, M., Dai, S., Graham, I.T., Nechaev, V.P., French, D., Zhao, F., Shao, L., Liu, S., Zuo, J., Zhao, J., 2021. Mineralogical and geochemical characteristics of altered volcanic ashes (tonsteins and K-bentonites) from the latest Permian coal-bearing strata of western Guizhou Province, southwestern China. *Int. J. Coal Geol.* 237, 103707.
- Spears, D.A., 2012. The origin of tonsteins, an overview, and links with seatearths, fireclays and fragmental clay rocks. *Int. J. Coal Geol.* 94, 22–31.
- Spears, D., Arbusov, S., 2019. A geochemical and mineralogical update on two major tonsteins in the UK Carboniferous Coal Measures. *Int. J. Coal Geol.* 210, 103199.
- Spears, D., Kanaris-Sotiriou, R., 1979. A geochemical and mineralogical investigation of some British and other European tonsteins. *Sedimentology* 26, 407–425.
- Spears, D., Duff, P.M.D., Caine, P., 1988. The West Waterberg tonstein, South Africa. *Int. J. Coal Geol.* 9, 221–233.
- Sutherland, L., Graham, I., Yaxley, G., Armstrong, R., Giuliani, G., Hoskin, P., Nechaev, V., Woodhead, J., 2016. Major zircon megacryst suites of the Indo-Pacific lithospheric margin (ZIP) and their petrogenetic and regional implications. *Mineral. Petrol.* 110 (2), 399–420.
- Taylor, J.C., 1991. Computer programs for standardless quantitative analysis of minerals using the full powder diffraction profile. *Powder Diffract* 6, 2–9.
- Taylor, S.R., McLennan, S.M., 1985. The Continental Crust: Its Composition and Evolution. Blackwell, London, 312 pp.
- Triplehorn, D.M., Bohor, B.F., 1981. Altered Volcanic Ash Partings in the C Coal Bed, Ferron Sandstone Member of the Mancos Shale, Emery County, Utah. US Geological Survey Open-file Report 81-775. 44 p.
- Triplehorn, D.M., Turner, D.L., Naeser, C.W., 1977. K-Ar and fission-track dating of ash partings in coal beds from the Kenai Peninsula, Alaska: A revised age for the Homerian Stage–Clamgulchian Stage boundary. *Geol. Soc. Am. Bull.* 88, 1156–1160.
- Turner, D.L., Frizzell, V.A., Triplehorn, D.M., Naeser, C.W., 1983. Radiometric dating of ash partings in coal of the Eocene Puget Group, Washington: Implications for paleobotanical stages. *Geology* 11, 527–531.
- Wainman, C., McCabe, P., Crowley, J., Nicoll, R., 2015. U-Pb zircon age of the Walloon Coal Measures in the Surat Basin, southeast Queensland: implications for paleogeography and basin subsidence. *Aust. J. Earth Sci.* 62, 807–816.
- Wang, W., Tang, J., Xu, W.-L., Wang, F., 2015. Geochronology and geochemistry of Early Jurassic volcanic rocks in the Erguna Massif, northeast China: Petrogenesis and implications for the tectonic evolution of the Mongol–Okhotsk suture belt. *Lithos* 218, 73–86.
- Wang, X., Wang, X., Pan, S., Yang, Q., Hou, S., Jiao, Y., Zhang, W., 2018. Occurrence of analcime in the middle Jurassic coal from the Dongsheng Coalfield, northeastern Ordos Basin, China. *Int. J. Coal Geol.* 196, 126–138.
- Wang, M., Zhong, Y.-T., He, B., Denysyn, S.W., Wang, J., Xu, Y.-G., 2020. Geochronology and geochemistry of the fossil-flora-bearing Wuda Tuff in North China Craton and its tectonic implications. *Lithos* 364, 105485.
- Ward, C.R., 2002. Analysis and significance of mineral matter in coal seams. *Int. J. Coal Geol.* 50, 135–168.
- Wesolowski, D.J., 1992. Aluminum speciation and equilibria in aqueous solution: I. The solubility of gibbsite in the system Na-K-Cl-OH-Al (OH) 4 from 0 to 100 C. *Geochim. Cosmochim. Acta* 56, 1065–1091.
- Winchester, J.A., Floyd, P.A., 1977. Geochemical discrimination of different magma series and their differentiation products using immobile elements. *Chem. Geol.* 20, 325–343.
- Wu, Y.-D., Yang, J.-H., Wang, H., Zhu, Y.-S., Xu, L., Zhou, B.-Q., Li, R., 2021. Origin and tectonic implications of Early Cretaceous Siziwangqi volcanic rocks from the North China Craton. *Lithos* 400, 106431.
- Yang, F., Santosh, M., Kim, S.W., 2018. Mesozoic magmatism in the eastern North China Craton: Insights on tectonic cycles associated with progressive craton destruction. *Gondwana Res.* 60, 153–178.
- Zaritsky, P., 1985. A review of the study of tonsteins in the Donets basin: Congrès International de Stratigraphie et Géologie du Carbonifère, 10th, Madrid, 1983. *Compt. Rendus* 4, 235–241.
- Zhang, S., Zhao, Y., Davis, G.A., Ye, H., Wu, F., 2014. Temporal and spatial variations of Mesozoic magmatism and deformation in the North China Craton: Implications for lithospheric thinning and decratonization. *Earth Sci. Rev.* 131, 49–87.
- Zhang, Z., Wang, C., Lv, D., Hay, W.W., Wang, T., Cao, S., 2020. Precession-scale climate forcing of peatland wildfires during the early middle Jurassic greenhouse period. *Glob. Planet. Chang.* 184, 103051.
- Zhang, Z., Wang, T., Ramezani, J., Lv, D., Wang, C., 2021. Climate forcing of terrestrial carbon sink during the Middle Jurassic greenhouse climate: chronostratigraphic analysis of the Yan'an Formation, Ordos Basin, North China. *Geol. Soc. Am. Bull.* 133, 1723–1733.
- Zhao, L., Ward, C.R., French, D., Graham, I.T., 2012. Mineralogy of the volcanic-influenced Great Northern coal seam in the Sydney Basin, Australia. *Int. J. Coal Geol.* 94, 94–110.
- Zhao, L., Ward, C.R., French, D., Graham, I.T., 2015. Major and trace element geochemistry of coals and intra-seam claystones from the Songzao Coalfield, SW China. *Minerals* 5, 870–893.
- Zhao, L., Dai, S., Graham, I.T., Li, X., Liu, H., Song, X., Hower, J.C., Zhou, Y., 2017. Cryptic sediment-hosted critical element mineralization from eastern Yunnan Province, southwestern China: mineralogy, geochemistry, relationship to Emeishan alkaline magmatism and possible origin. *Ore Geol. Rev.* 80, 116–140.
- Zheng, X., Dai, S., Nechaev, V., Sun, R., 2020. Environmental perturbations during the latest Permian: evidence from organic carbon and mercury isotopes of a coal-bearing section in Yunnan Province, southwestern China. *Chem. Geol.* 549, 119680.
- Zhou, Y., Bohor, B.F., Ren, Y., 2000. Trace element geochemistry of altered volcanic ash layers (tonsteins) in Late Permian coal-bearing formations of eastern Yunnan and western Guizhou Provinces, China. *Int. J. Coal Geol.* 44, 305–324.
- Zielinski, R.A., 1985. Element mobility during alteration of silicic ash to kaolinite—a study of tonstein. *Sedimentology* 32, 567–579.
- Ziemniak, S., Jones, M., Combs, K., 1993. Solubility behavior of titanium (IV) oxide in alkaline media at elevated temperatures. *J. Solut. Chem.* 22, 601–623.